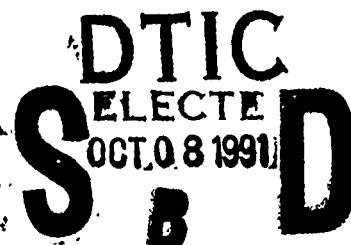# REPRESENTING THE NOMINAL PATH FOR AN INTERIOR LIBRATION POINT ORBIT IN THE SUN-EARTH+MOON ELLIPTIC RESTRICTED THREE-BODY PROBLEM

STEVEN C. GORDON, LT COL, USAF

DEPT OF MATHEMATICAL SCIENCES

SEPTEMBER 1991

FINAL REPORT

DTIC
ELECTE
OCT.0 8 1991
S D
B

91-12557

REPORT DOCUMENTATION PAGE

1. AGENCY USE ONLY (Leave blank)	2. REPORT DATE 7 Sep 1991	3. REPORT TYPE AND DATES COVERED Final

4. TITLE AND SUBTITLE
Representing the Nominal Path For an Interior Libration Point Orbit in the Sun-Earth+Moon Elliptic Restricted Three-Body Problem

5. FUNDING NUMBERS
PR 37731G

6. AUTHOR(S)

Steven C. Gordon, Lt Col, USAF

7. PERFORMING ORGANIZATION NAME(S) AND ADDRESS(ES)

Department of Mathematical Sciences
United States Air Force Academy, Colorado 80840

8 PERFORMING ORGANIZATION REPORT NUMBER

USAFATR 91-11

9. SPONSORING/MONITORING AGENCY NAME(S) AND ADDRESS(ES)

Frank J. Seiler Research Laboratory
United States Air Force Academy, Colorado 80840

10. SPONSORING/MONITORING AGENCY REPORT NUMBER

11. SUPPLEMENTARY NOTES
Research conducted under the direction of Prof K. C. Howell, School of Aeronautics and Astronautics, Purdue University

12a. DISTRIBUTION/AVAILABILITY STATEMENT

12b. DISTRIBUTION CODE

13. ABSTRACT (Maximum 200 words)

Bounded nominal paths can be constructed in the vicinity of the interior equilibrium point (sometimes called a libration or Lagrange point) for the Sun-Earth+Moon Elliptic Restricted Three-Body Problem. Numerical integration is used to generate the periodic or quasi-periodic reference trajectories in this effort. The output of the routine will be numerical values for each of the six states (three position and three velocity) at each of the integration time steps. Linearization of both the equations of motion and of the equations representing the tracking solution assumes access to a continuous representation of the spacecraft's orbit. Follow-on research that investigates tracking errors or station-keeping costs may also need a continuous (and smooth) representation of the six states or, at least, may need access to an interpolation routine. Consequently, this work explores the generation of curves through the numerical data representing the libration point orbits in the Sun-Earth+Moon ER3BP; these orbits are computed in the vicinity of the interior libration point between the Sun and the Earth+Moon barycenter.

14. SUBJECT TERMS
Curve fitting, libration points, three-body problem, least squares, cubic splines, spacecraft orbits

15. NUMBER OF PAGES
59

16. PRICE CODE

17. SECURITY CLASSIFICATION OF REPORT	18. SECURITY CLASSIFICATION OF THIS PAGE	19. SECURITY CLASSIFICATION OF ABSTRACT	20. LIMITATION OF ABSTRACT
UNCLASSIFIED	UNCLASSIFIED	UNCLASSIFIED	

USAFA-TR-91-11

Technical Review by Captain Rich Schooff
Department of Mathematical Science
USAFA Academy, Colorado 80840

Technical Review by Lt Col Daryl G. Boden
Department of Astronautics
USAF Academy, Colorado 80840

Editorial Review by Lt Col Donald C. Anderson
Department of English
USAF Academy, Colorado 80840

This research report entitled "Representing The Nominal Path
For An Interior Libration Point Orbit In The Sun-Earth+Moon
Elliptic Restricted Three-Body Problem" is presented as a
competent treatment of the subject, worthy of publication. The
United States Air Force Academy vouches for the quality of the
research, without necessarily endorsing the opinions and
conclusions of the author.

This report has been cleared for open publication and public
release by the appropriate Office of Information in accordance
with AFM 190-1, AFR 12-30, and AFR 80-3. This report may have
unlimited distribution.

Robert K. Morrow, Jr.

ROBERT K. MORROW JR., Lt Col, USAF   *28 Oct 91*
Director of Research   Dated

REPRESENTING THE NOMINAL PATH FOR
AN INTERIOR LIBRATION POINT ORBIT
IN THE SUN-EARTH+MOON ELLIPTIC
RESTRICTED THREE-BODY PROBLEM

Lieutenant Colonel Steven C. Gordon,

Assistant Professor

Department of Mathematical Sciences

PREFACE

Bounded nominal paths can be constructed in the vicinity of the interior equilibrium point (sometimes called a libration or Lagrange point) for the Sun-Earth+Moon Elliptic Restricted Three-Body Problem. The nominal paths may be computed using an analytic approximation or, more accurately, using a numerical integration routine. Numerical integration is used to generate the periodic or quasi-periodic reference trajectories in this effort. The output of the routine will be numerical values for each of the six states (three position and three velocity) at each of the integration time steps. Linearization of both the equations of motion and of the equations representing the tracking solution assumes access to a continuous representation of the spacecraft's orbit. Follow-on research that investigates tracking errors or station-keeping costs may also need a continuous (and smooth) representation of the six states or, at least, may need access to an interpolation routine. Consequently, this work explores the generation of curves through the numerical data representing the libration point orbits in the Sun-Earth+Moon ER3BP; these orbits are computed in the vicinity of the interior libration point between the Sun and the Earth/Moon barycenter. This effort is supported by the Frank J. Seiler Research Laboratory and has been conducted as doctoral research under the direction of Professor K.C. Howell, School of Aeronautics and Astronautics, Purdue University, West Lafayette, Indiana.

TABLE OF CONTENTS

LIST OF FIGURES

LIST OF TABLES

INTRODUCTION

With the expansion of space exploration programs worldwide, interest has increased in the design of innovative, complex, and yet low-cost spacecraft trajectories that meet demanding mission requirements. In most of the missions flown in the last few decades, the spacecraft spent the majority of the flight time in a force environment dominated by a single gravitational field. For the preliminary mission analysis in these cases, additional attracting bodies and other forces could be modeled, when required, as perturbing influences. Analysis of some recently proposed and more adventurous missions, such as those involving libration point orbits, will require dynamic models of higher complexity, since at least two gravitational fields are of nearly equal influence on the spacecraft throughout the majority of the mission. Thus, trajectories determined for a system consisting of numerous gravitational forces have been of particular theoretical and practical interest in recent years.

One type of many-body problem, motion within a three-body system of forces, has a wide range of applications. The general problem of three bodies assumes that each body has finite mass and that the motion is a result of mutual gravitational attraction. When the mass of one of the three bodies is assumed to be sufficiently small (infinitesimal) so that it does not affect the motion of the other two bodies (primaries) in the system, the "restricted three-body problem" results. The primaries can be further assumed to be moving in known elliptic or circular orbits about their common center of mass. Therefore, the elliptic restricted three-body problem, where the primaries are assumed to be in known elliptic orbits, may be considered a reasonably approximate model for a spacecraft moving within the gravitational fields of the Sun and the Earth, for instance.

In the formulation of the restricted three-body problem, one mass is defined as infinitesimal relative to the remaining two masses (primaries). The primaries, unaffected by the infinitesimal mass, move under their mutual gravitational attractions. In the elliptic restricted three-body problem (ER3BP), the primaries are assumed to move on elliptic paths. If the eccentricity of the primaries' orbit is assumed to be zero, the circular restricted three-body problem (CR3BP) results. Even for known primary motion, however, a general, closed-form solution for motion of the third body of infinitesimal mass does not exist. In the restricted three-body problem (ER3BP or CR3BP), five equilibrium (libration) solutions can be found. These equilibrium points, sometimes also called Lagrange points, are particular solutions of the equations of motion governing the path of the infinitesimal mass moving within the gravitational fields of the primaries.

The equilibrium points are defined relative to a coordinate system rotating with the primaries. At these locations, the forces on the spacecraft are in equilibrium. These forces include the gravitational forces from the massive bodies and the centrifugal force associated with the rotation of the system. (The addition of solar radiation pressure to the force model changes the locations of the five Lagrange points, although they can still be defined, and these solar radiation effects are discussed in Gordon[1].) The libration points are located in the plane of primary rotation. Three of the libration points are on the line between the two massive bodies, and one of these collinear points is interior to the primaries. The last two points are at the vertices of two equilateral triangles in the plane of primary rotation. The triangles have a common base that is the line between the primary masses.

For the CR3BP, the five libration points are stationary relative to the rotating reference frame. If the problem is generalized to the ER3BP, the libration points pulsate as the distance between the primaries varies with time. In both the circular and elliptic restricted problems, two-dimensional and three-dimensional trajectories, both periodic and quasi-periodic paths, can be computed in the vicinity of these libration points.

Three-dimensional, periodic "halo" orbits in the vicinity of the collinear libration points have been studied since the late 1960s. Early work concerning these orbits was motivated by studies related to exploring the far side of the Moon. These studies were completed in support of the planned Apollo 18 lunar exploration mission that was later canceled. Robert Farquhar coined the term "halo" to describe a three-dimensional, periodic orbit near a libration point on the far side of the Moon in the Earth-Moon system.[2] These orbits were designed to be large enough so that the spacecraft would be constantly in view of the Earth and would thus appear as a halo around the Moon. A communications station in this type of orbit could maintain constant contact between the Earth and a lunar experimentation station on the far side of the Moon.[3]

Quasi-periodic orbits near libration points are also currently of great research interest. The variations in size and shape that a quasi-periodic orbit can exhibit may add valuable flexibility for mission planning. This type of bounded, three-dimensional libration point trajectory is called a Lissajous orbit since specific planar projections of these quasi-periodic trajectories may look like a special type of "Lissajous" curve. Physicist Jules Antoine Lissajous (1822-1880) investigated curves that were generated by compounding simple harmonic motions at right angles, and he delivered a paper on this subject to the Paris Academy of Sciences in 1857. Nathaniel Bowditch of Salem, Massachusetts, had conducted some similar work in 1815. Lissajous curves have a wide variety of shapes that depend on the frequency, phase, and amplitude of the orthogonal components of the motion.[4,5] When the in-plane and the (orthogonal) out-of-plane frequencies of the linearized motion are nearly (but not) equal, the resulting path is typically called a Lissajous trajectory.

A method to generate approximations for this type of quasi-periodic orbital path was developed analytically by Farquhar and Kamel in 1973.[6] They derived a third-order approximate analytic solution for a translunar libration point orbit in the Earth-Moon ER3BP that also included solar gravity perturbations. In 1975, Richardson and Cary then developed a fourth-order analytic Lissajous approximation in the Sun-Earth+Moon barycenter system.[7] The notation "Earth+Moon"

3

indicates that the Earth and the Moon are treated as one body with mass center at the Earth-Moon barycenter. In consideration of the lunar perturbation, Farquhar has shown that the accuracy of solutions in the Sun-Earth CR3BP can be enhanced if the collinear libration points are defined along the line between the Sun and the center of mass of the Earth and the Moon.[8] Since 1975, a few researchers have considered methods to numerically generate Lissajous trajectories, but the lack of periodicity of a Lissajous path complicates numerical construction of bounded trajectories. Howell and Pernicka have developed a numerical technique for determination of three-dimensional, bounded Lissajous trajectories of arbitrary size and duration.[9-14]

The numerical integration routine computes bounded periodic or quasi-periodic libration point orbits. The numerical ouput (three position and three velocity states) is indexed by integration time steps; follow-on research may require a continuous representation of the orbit instead of a tabular listing of the numerical data. The first chapter briefly covers the background of the problem. The following chapter then discusses the four methods of curve fitting investigated and the method selected to be used in follow-on research.

4

CHAPTER 1: BACKGROUND

In this chapter, the elliptic restricted three-body problem and the associated coordinate systems are reviewed; the equations of motion for an infinitesimal mass moving in the gravity fields of two massive bodies are then presented. Next, locations of the libration points are discussed. Finally, the state transition matrix and the construction of bounded nominal orbits near the collinear Lagrange points are summarized. A more thorough discussion of these topics is presented in Gordon. [1]

A. Elliptic Restricted Three-Body Problem

The elliptic restricted three-body problem is a simplification of the general problem of three bodies. In the general three-body problem, each of the three bodies is assumed to be a particle of finite mass and, thus, exerts an influence on the motion of each of the other bodies. Neither the general nor the restricted problem of three bodies has a general closed-form solution. However, when problem simplifications are made, particular solutions can be determined. If the mass of one of the bodies is restricted to be infinitesimal, such that it does not affect the motion of the other two massive bodies (primaries), the restricted three-body model results. The primaries are assumed to be in known elliptic (ER3BP) or circular (CR3BP) orbits about their common mass center (barycenter). The problem can then be completely described by a single second-order vector differential equation with variables appropriately defined for a specified coordinate frame.

5

B. Coordinate Systems

The two standard coordinate systems used in the analysis of this problem have a common origin at the center of mass (barycenter) of the primaries. Primaries with masses m_1 and m_2 such that $m_1 \geq m_2$ are assumed here, although this distinction is arbitrary. The infinitesimal mass is denoted as m_3. These masses (m_1, m_2, m_3) correspond to particles situated at points P_1, P_2, and P_3, respectively. The barycenter is denoted as "B," and the resulting arrangement is shown in Figure 1-1. The rotating coordinate system is defined as $x_R y_R z_R$, and the inertial system is identified as $x_I y_I z_I$. Note that both coordinate systems are right-handed, and the x and y axes for both systems are in the plane of motion of the primaries. The x_I axis is, of course, assumed to be oriented in some fixed direction; in this specific formulation of the problem, it is assumed to be parallel to a vector defined with a base point at the Sun and directed toward periapsis of the Earth's orbit. The rotating x_R axis is defined along the line that joins the primaries and is directed from the larger toward the smaller primary. The z axes are coincident and are directed parallel to the primary system angular momentum vector. The y_R axis completes the right-handed $x_R y_R z_R$ system.

C. Equations of Motion

Newtonian mechanics are used to formulate the equations of motion for m_3 (the spacecraft) relative to B as observed in the inertial reference frame. The sum of the forces on m_3 resulting from both the gravity fields of masses m_1 (the Sun) and m_2 (the Earth-Moon barycenter) and from the solar radiation pressure can be used to produce the following second-order vector differential equation:

$$\bar{\rho}'' = -G\left(\frac{m_1}{d^3}\right)\bar{d} - G\left(\frac{m_2}{r^3}\right)\bar{r} + \left(\frac{kS}{d^3}\right)\bar{d}. \qquad (1-1)$$
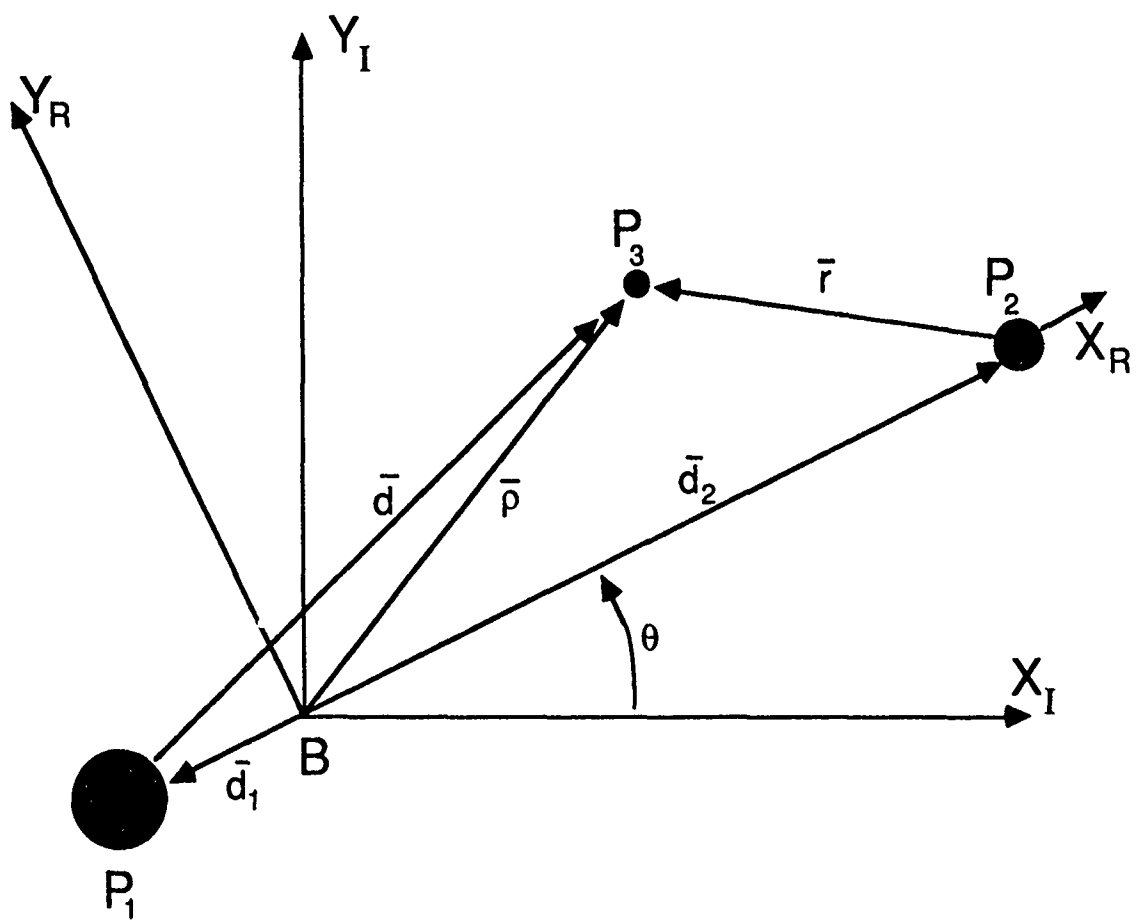
Figure 1-1. Coordinate Systems With Barycenter Origin.

The overbar denotes a vector, and primes indicate differentiation with respect to dimensional time. All quantities are dimensional, as appropriate, and the quantity "G" is the universal gravitiational constant. The scalars "d" and "r" in equation (1-1) denote the magnitudes of the vectors $\bar{d}$ and $\bar{r}$, respectively, as depicted in Figure 1-1. The dimensionless scalar "k" is the solar reflectivity constant, and "S" is the solar radiation pressure constant. The formulation of the solar radiation force model and the values for the solar radiation constants are derived from previous work by Bell.[15] The numerical values for these constants are selected from characteristic data for a spacecraft previously in a libration point orbit:

$$S = \frac{A\, S_0\, r_0^2}{c\, m_3}, \qquad (1-2)$$

where $k = 1.2561$, $S_0 = 1352.098$ kg/sec^3, $r_0 = 1.4959787 \times 10^8$ km, c = the speed of light $= 2.998 \times 10^8$ m/sec, A = surface area of the spacecraft's sun-facing side $= 3.55$ m^2, and m_3 = mass of the spacecraft = 435 kg. The constant S_0 is the solar light flux measured at one astronomical unit (A.U.), and r_0 is the nominal distance associated with the measurement of the solar flux S_0.[15] The value of A, also termed the effective cross-sectional area of the spacecraft, is considered to be constant in this work. The constant k is a material parameter dependent on the absorptivity of the spacecraft surface and is generally confined to a range of $0 \le k \le 2.0$.[15]

The position vector $\bar{\rho}$ is written in rotating components as

$$\bar{\rho} = x\, \hat{x}_R + y\, \hat{y}_R + z\, \hat{z}_R \qquad (1-3)$$

where $\hat{x}_R, \hat{y}_R, \hat{z}_R$ are unit vectors. The velocity and the acceleration of the spacecraft (particle P_3 with mass m_3) relative to the barycenter B as observed in the inertial reference frame can then be derived. The following kinematic expression for $\bar{\rho}''$ can be derived:

$$\bar{\rho}'' = (x''-\theta''y-2\theta'y'-\theta'^2x)\hat{x}_R+(y''+\theta''x+2\theta'x'-\theta'^2y)\hat{y}_R+z''\hat{z}_R. \qquad (1\text{-}4)$$

Notice that equation (1-4) includes terms with the angular velocity, $\theta'(t)$, and angular acceleration, $\theta''(t)$, of the rotating reference frame with respect to the inertial frame. By using known elliptic orbital elements, readily computed expressions for θ' and θ'' can be found:

$$\theta' = \frac{\sqrt{a(1-e)(1+e)} \ \sqrt{G(m_1+m_2)}}{a^2 \ (1 - e\cos(E))^2}. \qquad (1\text{-}5)$$

$$\theta'' = \frac{-2G(m_1+m_2)\sqrt{(1-e)(1+e)} \ e\sin(E)}{a^3(1 - e\cos(E))^4}. \qquad (1\text{-}6)$$

where e is the eccentricity, E is the eccentric anomaly, and a is the semi-major axis of the primary orbit.

Three scalar equations of motion for P_3 can be derived using the dimensional equations (1-1), (1-2), (1-4), (1-5), and (1-6); however, for convenience, the following scaling factors are typically introduced:

(1) The sum of the masses of the primaries equals one mass unit. ($m_1 + m_2 = 1$ unit of mass)

(2) The mean distance between the primaries equals one unit of distance. (a = 1 unit of distance)

(3) The universal gravitational constant is equal to one unit by proper choice of characteristic time. (characteristic time = $1/n_{mean}$; thus G = 1 unit)

The dimensional equations of motion can be simplified and scaled by introducing the characteristic quantities defined above and by

9

introducing the nondimensional mass ratio μ, "psuedo-potential" U, and the scaled solar radiation constant s:

$$\mu = \frac{m_2}{m_1 + m_2} \qquad (1\text{-}7)$$

and

$$U = \frac{(1-\mu)}{d} + \frac{\mu}{r} + \frac{1}{2}\,\dot{\theta}^2(x^2 + y^2) - \frac{k\,s}{d} \qquad (1\text{-}8)$$

where the dot denotes the derivative with respect to characteristic time. The scaled solar radiation constant, s, is derived from the dimensional radiation constant denoted as S in equation (1-2) and, by using the characteristic quantities described above, its value is calculated as $s = 6.206597029461384 \times 10^{-6}$ nondimensional units. Then, the vector magnitudes, "d" and "r," are written in terms of scaled quantities as:

$$d = [(x + \mu R)^2 + y^2 + z^2]^{1/2}, \qquad (1\text{-}9)$$

$$r = [(x - R + \mu R)^2 + y^2 + z^2]^{1/2}. \qquad (1\text{-}10)$$

The three scalar second-order differential equations that result can be written in terms of characteristic quantities as

10

$$\ddot{x} - 2\,\dot{\theta}\,\dot{y} = \frac{\partial U}{\partial x} + \ddot{\theta}\,y = U_x + \ddot{\theta}\,y, \qquad (1\text{-}11)$$

$$\ddot{y} + 2\,\dot{\theta}\,\dot{x} = \frac{\partial U}{\partial y} - \ddot{\theta}\,x = U_y - \ddot{\theta}\,x, \qquad (1\text{-}12)$$

$$\ddot{z} \qquad = \frac{\partial U}{\partial z} \qquad = U_z. \qquad (1\text{-}13)$$

The scaled equations for the angular velocity and angular acceleration of the rotating frame relative to the inertial frame also simplify:

$$\dot{\theta} = \frac{\sqrt{(1-e)(1+e)}}{(1 - e\,\cos(E))^2}, \qquad (1\text{-}14)$$

$$\ddot{\theta} = \frac{-2\sqrt{(1-e)(1+e)}\ e\,\sin(E)}{(1 - e\,\cos(E))^4}. \qquad (1\text{-}15)$$

If the primaries are assumed to be moving in a circular orbit, then $\ddot{\theta} = 0$, $R = \dot{\theta} = 1$, and equations (1-11), (1-12), (1-13) reduce to three scalar equations in the simplified form:

11

$$\ddot{x} - 2\dot{y} = \frac{\partial U}{\partial x} = U_x, \qquad (1\text{-}16)$$

$$\ddot{y} + 2\dot{x} = \frac{\partial U}{\partial y} = U_y, \qquad (1\text{-}17)$$

$$\ddot{z} \qquad = \frac{\partial U}{\partial z} = U_z. \qquad (1\text{-}18)$$

The scalar equations (1-11), (1-12), and (1-13) corresponding to the elliptic restricted problem or equations (1-16), (1-17), and (1-18) derived for the circular restricted problem can be used to locate the five libration points in the rotating reference frame.

D. Locations of the Lagrangian (Libration) Points

By using scalar equations (1-16), (1-17), and (1-18) for motion in the CR3BP, the locations of the stationary equilibrium points can be determined. Equations (1-11), (1-12), and (1-13) can be used to determine ratios of distances that are constant in the ER3BP; these ratios are related to the locations of libration points that have been defined in the ER3BP and that "pulsate" with respect to the rotating reference frame as the distance between the primaries varies with time.

1. The CR3BP

In the CR3BP, the five libration points are equilibrium points and are stationary with respect to the rotating coordinate frame, that is, they are locations at which the forces on the third body sum to zero. The arrangement of points and the corresponding nondimensional distances are depicted in Figure 1-2. Note that three of the libration

12

Figure 1-2. Lagrange Point Locations in the Scaled CR3BP.

points (L_1, L_2, L_3) are collinear with the primaries; one collinear point (L_1) is interior to the primaries. The remaining two points (L_4 and L_5) are located at the vertices of two equilateral triangles that are in the plane of primary rotation and that have a common base between the primaries.

In the CR3BP, the libration points are stationary in the rotating coordinate frame. Stationary points are defined as points at which the relative velocity and acceleration are zero, such that

$$\dot{x} = \dot{y} = \dot{z} = \ddot{x} = \ddot{y} = \ddot{z} = 0. \tag{1-19}$$

By using equations (1-19) in equations (1-16) through (1-18), the useful conditions $U_x = U_y = U_z = 0$ are found. The three collinear libration points can be readily located by further noting that $y = z = 0$ for the points located on the rotating x_R axis.

2. The ER3BP

Five libration points also exist in the ER3BP, but they are not stationary relative to the rotating frame; rather, the collinear points pulsate along the x_R axis, and the triangular points pulsate relative to both the x_R and the y_R axes as the distance between the primaries varies with time. The equilibrium solutions can be located by using equations (1-11) through (1-13) to find ratios of certain distances that are, in fact, constant in the problem. The collinear libration points in the ER3BP can be found by assuming $\dot{x} \neq 0$, $x \neq 0$, and $\dot{y} = \ddot{y} = \dot{z} = \ddot{z} = y = z = 0$. The relative locations of the libration points in the ER3BP are depicted in Figure 1-3.

14
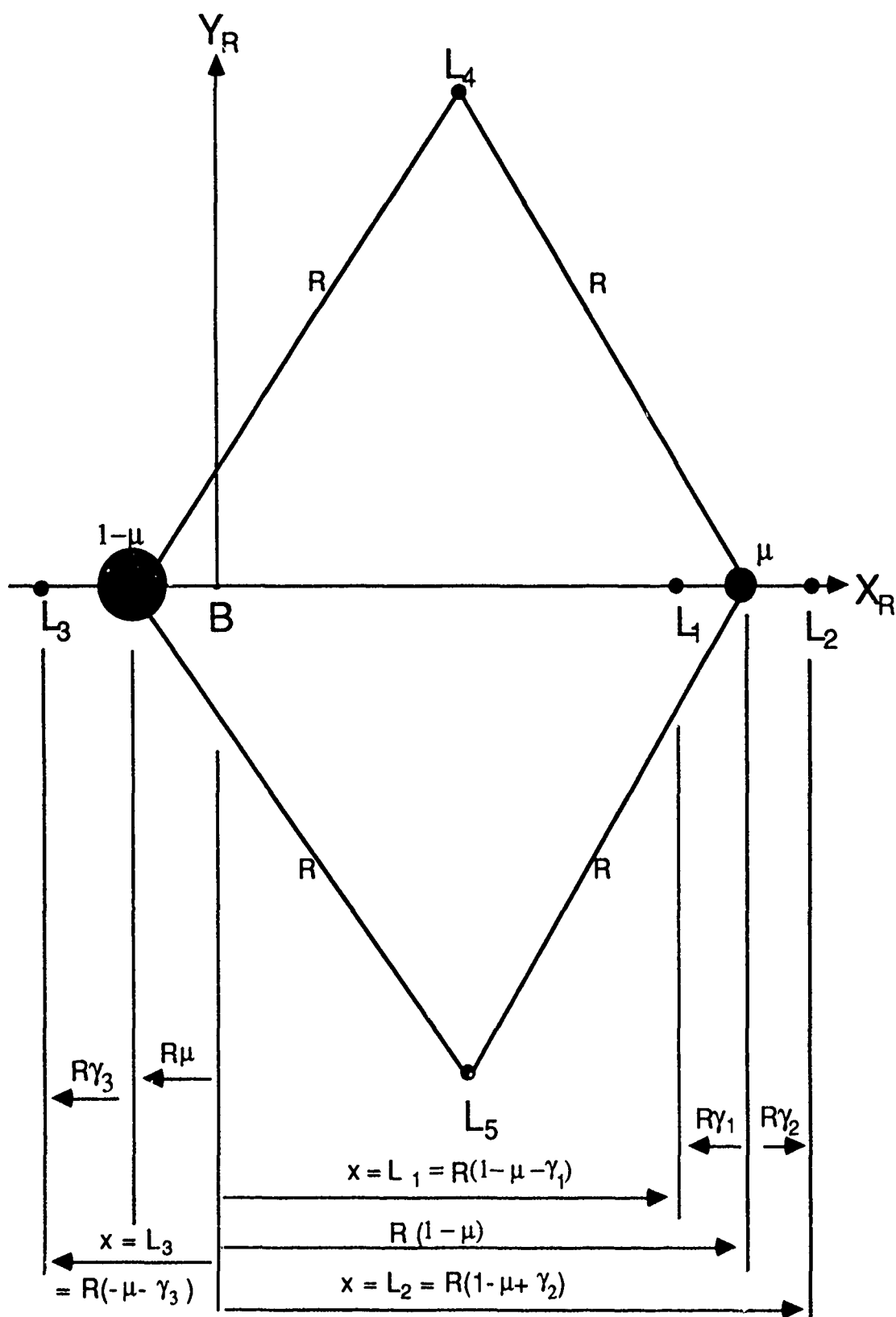
Figure 1-3. Lagrange Point Locations in the Scaled ER3BP.

15

E. State Transition Matrix

The state transition matrix is used in the calculation of the acceptable nominal trajectory, and it must also be available at varying time intervals along the nominal path for orbit determination error analysis investigations and station-keeping studies. The transition matrix is derived in connection with a linearizing analysis.

The equations of motion for the infinitesimal mass in the ER3BP can be linearized about a reference trajectory (nominal path) that is a solution of the differential equations. The states, three position and three velocity, and the state vector $\bar{x}$ are defined as

$$x_1 = x, \ x_2 = y, \ x_3 = z \ , \ x_4 = \dot{x}, \ x_5 = \dot{y}, \ x_6 = \dot{z}, \qquad (1-20)$$

and

$$\bar{x} = [x_1, \ x_2, \ x_3, \ x_4, \ x_5, \ x_6]^T. \qquad (1-21)$$

The reference trajectory is defined as $\bar{x}_{REF}$. Therefore, using a Taylor's series approach, the expansion about the reference path is written in the form of the first-order variational equation

$$\frac{d}{dt}(\tilde{x}) = \dot{\tilde{x}} = A(t) \ \tilde{x} \qquad (1-22)$$

where $\tilde{x} = \bar{x} - \bar{x}_{REF}$ is understood to be the vector of residuals relative to the nominal solution, and the matrix $A(t)$ contains the first-order terms in the Taylor's series expansion of the equations of motion about the nominal or reference solution of interest.

16

Using equations (1-11) through (1-13), A(t) can be expressed as

$$A(t) = \begin{bmatrix} 0 & I \\ U_{rr} + \ddot{\theta}\Omega & 2\dot{\theta}\Omega \end{bmatrix} \qquad (1\text{-}23)$$

where all four submatrices are dimension 3x3 and

$$U_{rr} = \begin{bmatrix} U_{xx} & U_{xy} & U_{xz} \\ U_{yx} & U_{yy} & U_{yz} \\ U_{zx} & U_{zy} & U_{zz} \end{bmatrix} \qquad (1\text{-}24)$$

with

$$\Omega = \begin{bmatrix} 0 & 1 & 0 \\ -1 & 0 & 0 \\ 0 & 0 & 0 \end{bmatrix}.$$

In equation (1-24), the notation is simplified for the partial derivatives; for instance

$$\frac{\partial^2 U}{\partial x^2} = U_{xx}.$$

The matrix A(t) can then be evaluated along the reference trajectory.

The vector differential equation (1-22) governing the state variations from the nominal path has a solution of the form

17

$$\tilde{x}(t) = \Phi(t,t_0) \, \tilde{x}(t_0) \tag{1-25}$$

where $\Phi(t,t_0)$ is the state transition matrix at time "t" relative to time "t_0." The matrix Φ, then, represents the sensitivities of the states at time "t" to small changes in the initial conditions. It is determined by numerically integrating the matrix differential equation

$$\frac{d}{dt} \, \Phi(t,t_0) = \dot{\Phi}(t,t_0) = A(t) \, \Phi(t,t_0), \tag{1-26}$$

with initial conditions $\Phi(t_0,t_0) = I$, the 6x6 identity matrix. Thus, the nonlinear equations of motion in (1-11) through (1-13) and the matrix equation (1-26) combine to result in 42 first-order differential equations that can be simultaneously integrated numerically to determine the state vector and its associated transition matrix at any instant of time. The reference trajectories that are of interest in this research are generated by a numerical integration method that uses a differential corrections process developed by Howell and Pernicka.[9-14] The orbits include solar radiation pressure forces as formulated by Bell[15] specifically for an orbit associated with the interior Lagrange point in the Sun-Earth system. The numerical integration routines used in this work are fourth- and fifth-order Runge-Kutta formulas available in the 386-Matlab software package.[16]

F. Bounded Orbits Near Libration Points

The computation of bounded periodic and quasi-periodic orbits in the vicinity of libration points has been of increasing interest during the past 100 years. This section first discusses the stability of the libration points in the CR3BP and the ER3BP. The construction of bounded orbits near the collinear Lagrange points is then summarized. Finally, the specific reference trajectories used in the orbit determination error analysis and station-keeping studies in this work are introduced.

1. Stability of the Libration Points in the CR3BP

The accomplishments of those researchers who have constructed bounded orbits near collinear libration points are particularly significant because the collinear points are considered "unstable" points of equilibrium but with (only) one mode producing positive exponential growth. Bounded motion in their vicinity, therefore, is determined by deliberately not exciting the unstable mode. A second mode produces negative exponential orbital decay and is also deliberately not excited. In the CR3BP, the remaining four eigenvalues are purely imaginary. The existence of initial conditions that result in only trigonometric (sinusoidal) functions as solutions means that the collinear libration points, while unstable, possess *conditional* stability (with proper choice of initial conditions) in the linear sense.[17]

The triangular libration points are marginally stable in the linear sense for a specific range of primary mass ratio in the CR3BP. Purely imaginary roots in two conjugate pairs are obtained for $\mu \leq .0385$, which is given here to four decimal places and is sometimes referred to as Routh's value.[18] The mass ratios (listed here to three decimal places), for example, in the three-body systems of the Earth-Moon ($\mu = 1.216 \times 10^{-6}$), Sun-Earth+Moon ($\mu = 3.022 \times 10^{-6}$) and Sun-Jupiter ($\mu = 9.485 \times 10^{-4}$) all satisfy the mass ratio requirement for marginal stability of the triangular points in the linearized model. Natural satellites, such as the Trojan asteroids or a moon of Saturn, occupy linearly stable orbits near triangular libration points in their respective systems.

2. Stability of the Libration Points in the ER3BP

Several researchers have analyzed the stability of the libration points in the elliptic problem, where both the mass ratio, μ, and the primary orbit eccentricity, e, influence stability.[17-21] The

instability of the collinear libration points as determined in the circular problem for all the values of mass parameter persists for the elliptic problem; an analysis of the collinear points shows instability for any combination of the values of both μ and e.

The results of a linearized stability analysis regarding the effects of eccentricity and mass ratio on the linear stability of the triangular points have been published by Danby[20] and then later by Bennett[21]. Both Danby and Bennett have numerically generated graphic depictions of the linear stability region in the μ-e plane. For the eccentricity in the Sun-Earth+Moon ER3BP, the value of μ which ensures linear stability is only slightly less than Routh's value (decreased by approximately one percent). An interesting aspect of the μ-e stability region is that a range of values of μ greater than Routh's value also defines a region of linear stability for a specific range of values of e less than .3143.

3. Construction of Bounded Collinear Libration Point Orbits

The initial goal in the process of generating bounded orbits near a collinear (unstable) libration point is to avoid exciting the unstable mode associated with the linearized motion. The meteoric dust particles that may be orbiting near Lagrange point L_2 in the Sun-Earth system could only linger near that point if they arrive with the "correct" initial position and velocity states relative to L_2. The "correct" initial conditions will only (primarily) excite the stable modes associated with the linearized motion and not (or minimally) excite the unstable mode. The degree to which the unstable mode is excited will determine the length of time that the dust particles linger near L_2.

The third-order analytic representation is used in this work to provide the initial model for the trajectories. The method of successive approximations, using the linearized solution as the first approximation to the nonlinear orbital path, and the method of dual time scales are used to derive the third-order result.[6,7,22] The method of successive approximations is used to generate an asymptotic

series in an appropriately small parameter. (The square root of the eccentricity of the primary orbit, that is the orbit of the Earth-Moon barycenter about the Sun, is the small parameter used here.) The method of dual time scales is used to convert the system of ordinary differential equations into a system of partial differential equations. In general, the method of multiple scales allows the various nonlinear resonance phenomena to be included in the approximate analytic solution and provides a method to remove secular terms. (Here, "secular" refers to terms that include the time variable and is derived from the French "siècle" meaning century.)

The analytic solution of Richardson and Cary[7] for the Sun-Earth+Moon ER3BP has been derived to fourth order, but the third-order approximation is found to be sufficient for this research.[9-14] A numerical integration algorithm, using a differential corrections procedure that is designed to adjust the first guess as obtained from the analytic approximation, can then be used to numerically generate the orbit of interest. A method developed by Howell and Pernicka[9-14] is used here to generate the orbital paths. Their method initially employs the approximate analytic solution to compute target points. A two-level (position matching then velocity matching), multi-step differential corrections algorithm is used to construct a numerically integrated, bounded trajectory that is continuous in position and velocity. A solar radiation pressure model developed by Bell[15] is also incorporated in the numerical integration procedure.

The method of Howell and Pernicka, including solar radiation pressure, uses an initial analytic guess that represents a halo orbit or, alternatively, a considerably smaller Lissajous path. The higher-order terms tend to slightly alter the first-order periodic or quasi-periodic pat'. Consequently, the initial target path for a halo orbit will generally not be precisely periodic. The two-level, multi-step differential corrections procedure then adjusts the initial analytic target orbit and, therefore, will compute a halo-type orbit that is nearly (but not exactly) periodic.

4. The Reference Paths Generated for This Work

Precisely periodic halo orbits exist in the CR3BP. They also exist in the ER3BP, but, in the ER3BP, they are multiple revolution trajectories with periods much longer than those of interest here. Nearly periodic orbits are more practical in the ER3BP and are much more likely to be used in mission planning; therefore, the goal here should be slightly modified to be the comparison of Lissajous and "halo-type" orbits. The general shapes of the three-dimensional halo-type and Lissajous orbits can be seen by plotting three orthographic views of each orbit, using the tabular data from the numerical integration routine. Figure 1-4 depicts three orthographic views of point plots for the Lissajous orbit used in this research. Figure 1-5 contains three orthographic views (on a slightly different scale) of the considerably larger halo-type orbit. (Note that, in general, the amplitude ratio for Lissajous trajectories is arbitrary. In halo orbits, however, constraining the amplitude ratio results in equalized frequencies for in-plane and out-of-plane motion.) The orbits are depicted in the rotating reference frame centered at L_1.

Both orbits are clearly not periodic; a Lissajous orbit is often called a quasi-periodic path, and these two orbits could clearly be termed quasi-periodic or Lissajous paths. The major difference between the orbits is the larger size of the halo-type orbit; however, other differences are also present. The maximum x and y excursions of the halo-type orbit are approximately four times as large as those of the Lissajous path. Furthermore, the direction of motion (clockwise versus counterclockwise), as viewed in the y-z orthographic depiction, is different for the two orbits used here. The direction of motion on the halo-type orbit is counterclockwise in the y-z depiction; the direction of motion is clockwise in the y-z depiction for the Lissajous path. (Both orbits include clockwise motion in the x-y depiction.)

The two orbits can also be differentiated in terms of the direction of the maximum z excursion in the x-z depiction. If the maximum z excursion is in the positive z direction, the orbit can be termed a member of a "northern family" of orbits. When the maximum z excursion of the orbit is in the negative z direction, the orbit is

22
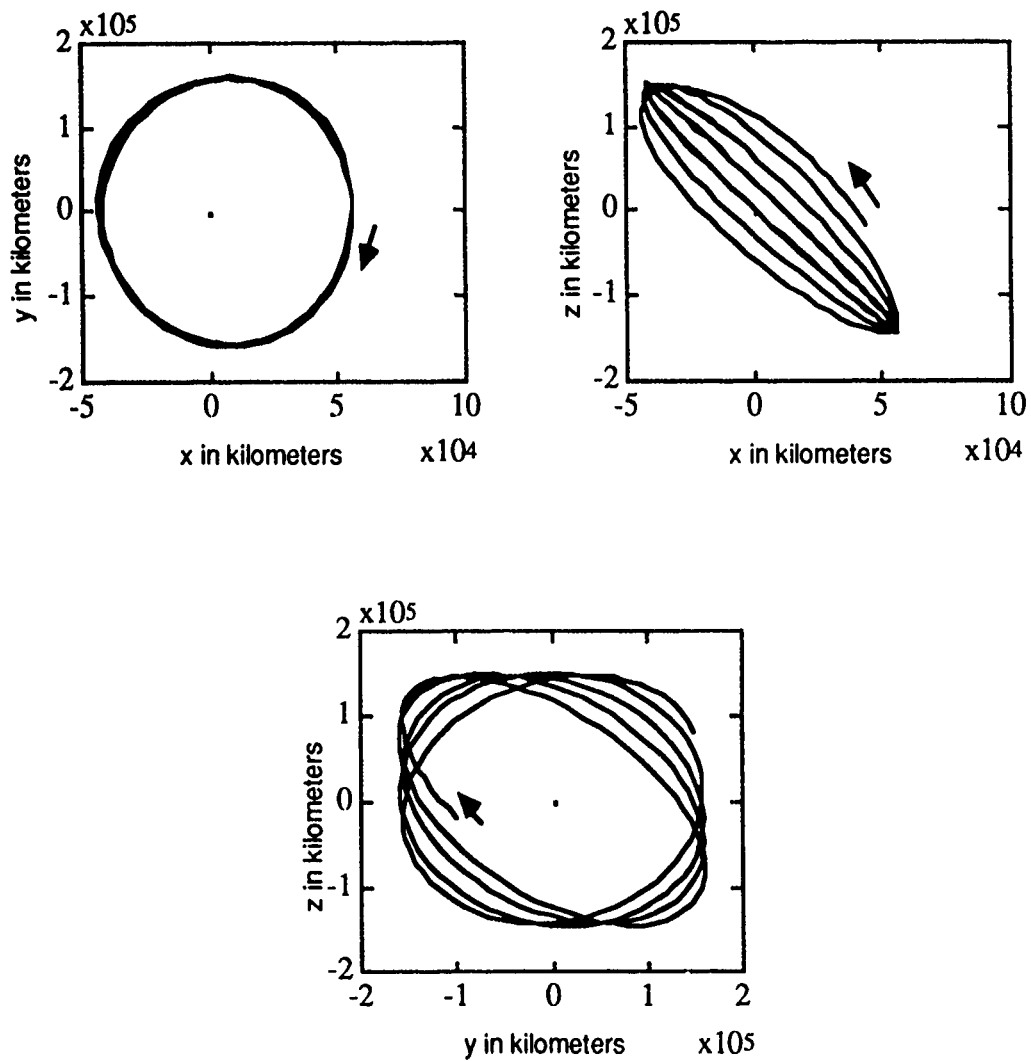
Indicates the direction of motion.

Indicates the location of the libration point.

Figure 1-4. Three Orthographic Views of a Lissajous Orbit.
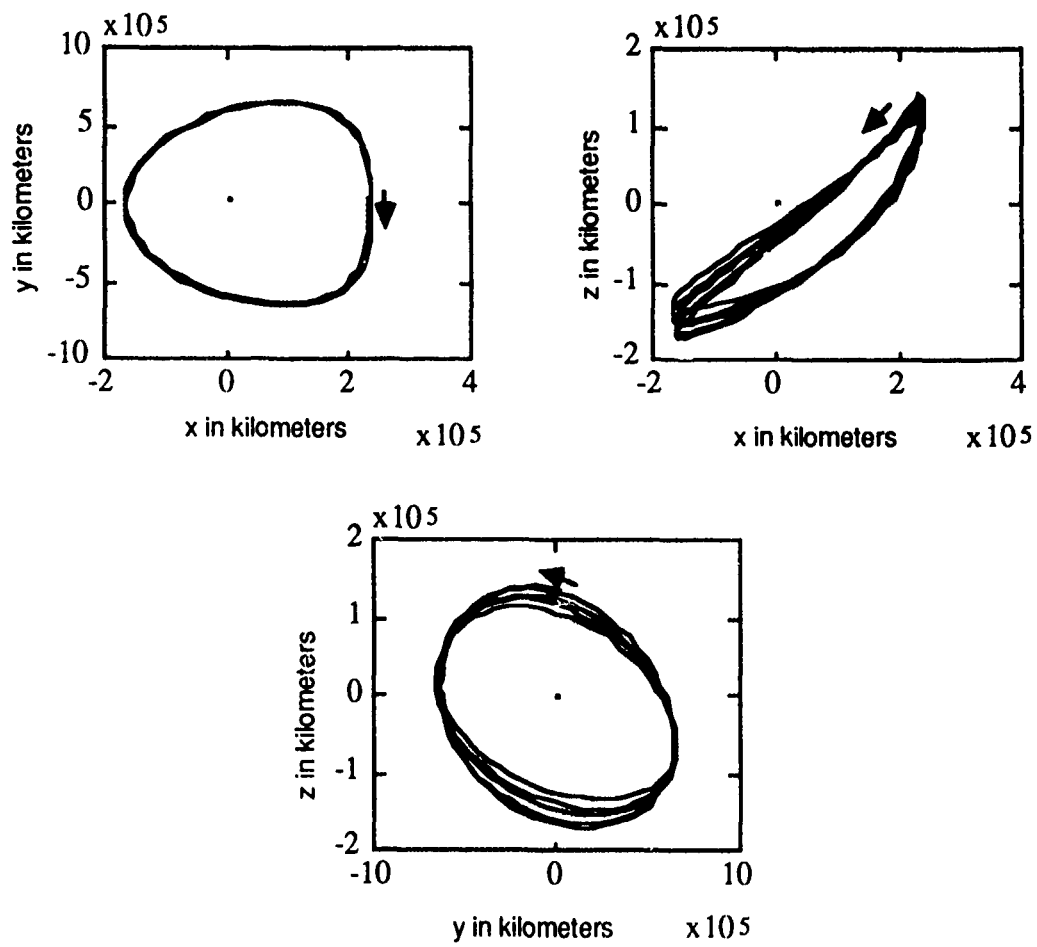
indicates direction of motion.

indicates the libration point location.

Figure 1-5. Three Orthographic Views of a Halo-Type Orbit.

24

termed a member of a "southern family" of orbits. In the x-z orthographic depiction, the smaller (Lissajous) path can be seen to be a member of a northern family of orbits, while the halo-type orbit is a member of a southern family of orbits.

Future work with these two orbits will include studies that generally require access to a nominal path that is at least piecewise smooth. Some method of curve fitting the numerically integrated data must consequently be investigated, and the evaluation of various methods can add valuable problem insight.

CHAPTER 2: CURVE FITTING THE NOMINAL PATH

The reference solution used in this research is generated by numerical integration of the nonlinear equations of motion. In one study, an investigation that used a consistent dynamic model for all comparisons, Richardson[8] has shown that a slight reduction in fuel expenditure can be realized if a numerically integrated, rather than an approximate analytic, nominal path is computed. The numerical integration method developed by Howell and Pernicka[9-14] is used here to generate a set of reference points for both position (three states) and velocity (three states), relative to the libration point of interest, at specified times. Time series point plots of all six state variables for approximately a 2-year segment of a Lissajous orbit are depicted in Figures 2-1 (position states) and 2-2 (velocity states). The method computes numerical data for the six states in a reference frame that is centered at the libration point (in this case L_1) and that rotates with the primaries. However, state estimation techniques and station-keeping algorithms considered in follow-on research require access to a continuous nominal path, rather than point plots, of acceptable accuracy.

The reference trajectory, represented as a (piecewise) smooth curve, could be constructed, approximately or exactly, through the points obtained from the numerical integration routine. The work here assumes that a curve that passes through the numerical data (exactly) is preferred. The effort required to generate a numerical solution, including forces modeled consistent with the ER3BP (or even more accurately modeled with ephemeris data) would seem to be wasted if the reference curve deviates too far from the numerical data. However, a method that approximates a smooth curve through the points is also desirable; that is, linear interpolation between the numerical data
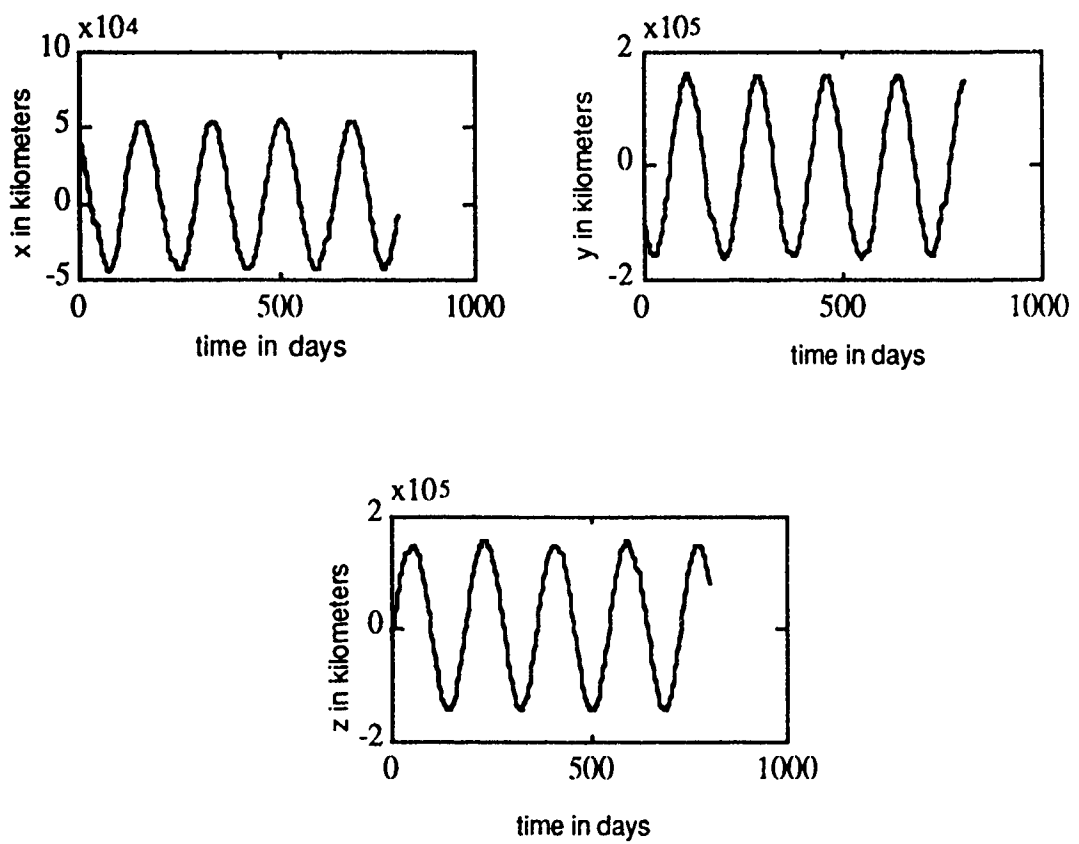
26

Figure 2-1. Time Series Plots of Three Lissajous Position States.
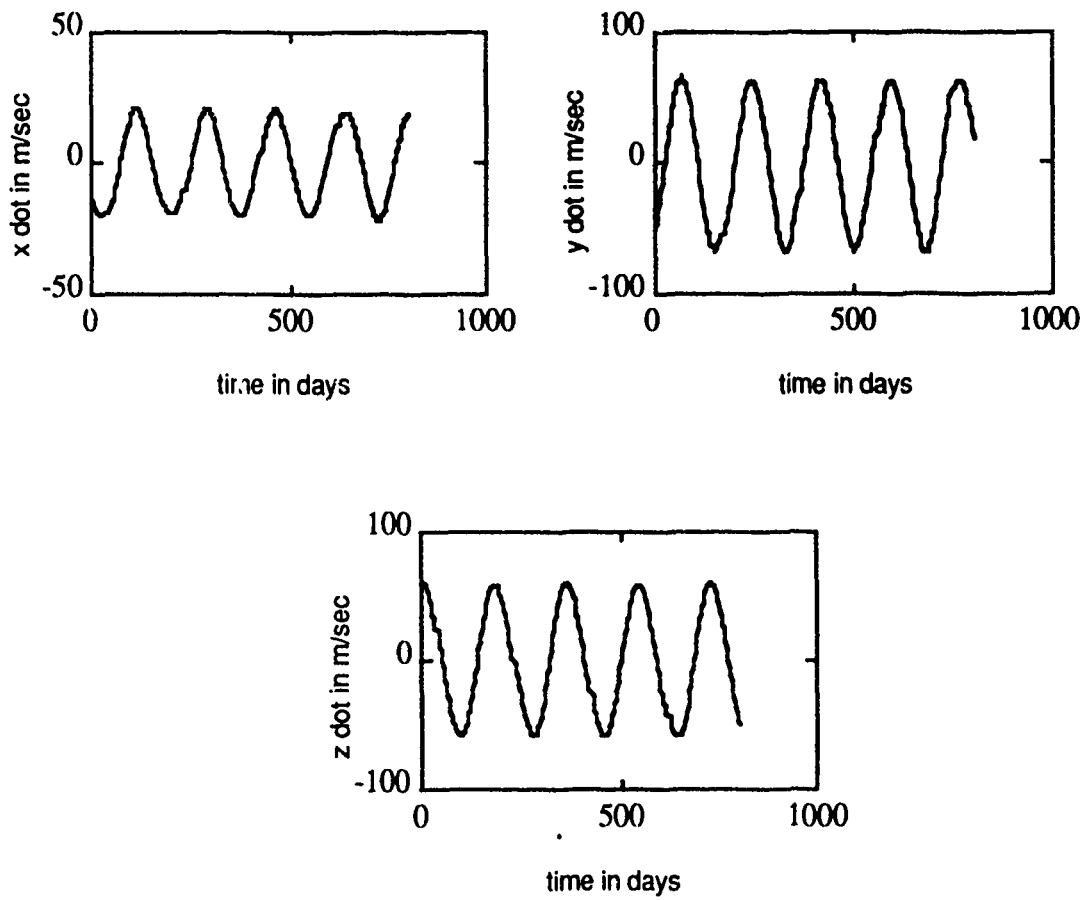
27

Figure 2-2. Time Series Plots of Three Lissajous Velocity States.

28

points was not considered acceptable. In one study, Pernicka[12] found that station-keeping costs for a libration point orbit were, in fact, sensitive to the accuracy of the curve fit. Clearly, a piecewise linear curve fit could not accurately match the concavity of the actual orbital path between data points, regardless of the size of the time steps used in the numerical integration routine.

Four methods of generating a curve for the nominal trajectory have been evaluated: Fourier series, least squares, weighted least squares, and cubic splines. The states associated with a quasi-periodic path were thought to be the most difficult to curve fit; therefore, various Lissajous trajectories were used to evaluate the curve-fitting methods. One of these methods is then selected to be used for the reference trajectory in follow-on state estimation and station-keeping research

A. Integrated Fourier Series

Joseph Fourier (1768-1830) solved heat flow problems using the method of separation of variables, and this application led to the development of the Fourier series.[3] Leonhard Euler and Alexis-Claude Clairaut (1713-1765) had already expanded some functions in such series representations and had obtained the general integral equations for the coefficients. Much earlier, the Babylonians had actually used a rudimentary form of a Fourier series for estimation problems.[36] However, Fourier made the crucial observation that every function could be so represented even if the function was not periodic or not even continuous.[23] Richardson[8,22] used numerically integrated Fourier series to represent the three position coordinates corresponding to a halo orbit (near L_1 in the Sun-Earth system). Richardson's work, and the periodic or quasi-periodic nature of the orbits that require a curve fit, made the initial investigation of Fourier series representations seem natural.

The three position and three velocity variables can be expressed parametrically as

$$x = x(t), \ y = y(t), \ z = z(t), \ \dot{x} = \dot{x}(t), \ \dot{y} = \dot{y}(t), \ \dot{z} = \dot{z}(t), \qquad (2\text{-}1)$$

and the plotted time history of the numerical value of each variable, as seen in Figures 2-1 and 2-2, reveals approximately sinusoidal behavior. (The dot denotes the derivative with respect to time.) The six states can be expressed in separate Fourier series, or the expressions for the three velocity states can be computed from the first time derivatives of the series expressions for the position variables. Richardson[8,22] used the latter method to find series representations for the velocity components corresponding to a libration point halo orbit. Similar techniques have also been used for a Lissajous path.

Studies by Howell and Pernicka have used numerically integrated Fourier coefficients for parameterized series expressions for the $x=x(t)$, $y=y(t)$, and $z=z(t)$ coordinates of position in a Lissajous orbit.[13,14] The series coefficients are integrated concurrently with the equations of motion.

For example, the coefficients for the x position series representation would be computed using

$$x(t) = \frac{a_0}{2} + \sum_{i=1}^{n} [a_i \cos(\frac{i\pi t}{L}) + b_i \sin(\frac{i\pi t}{L}),\qquad(2\text{-}2)$$

where

$$a_i = \frac{1}{L} \int_0^{2L} x(t) \cos(\frac{i\pi t}{L}) \, dt, \quad i = 0, 1, 2, \ldots, n\qquad(2\text{-}3)$$

and

$$b_i = \frac{1}{L} \int_0^{2L} x(t) \sin(\frac{i\pi t}{L}) \, dt, \quad i = 0, 1, 2, \ldots, n.\qquad(2\text{-}4)$$

The variable "L" is selected such that 2L is the duration of the orbit. (The duration of the orbit is sometimes referred to in this work as the

"fundamental period.") The variable "n" determines the number of terms retained in the series; for instance, when n = 16 and when a_0 is assumed to be zero, the resulting series representation for x(t) will have 2n = 32 terms. Note that there must also be series representations for y(t) and z(t). (There may also be series representations for velocities $\dot{x}(t)$, $\dot{y}(t)$, and $\dot{z}(t)$, or time derivatives of the Fourier series representations of the position states may be used, depending on the method selected.) The Fourier series coefficient equations are numerically inte_-ated along with the equations of motion (1-11) through (1-13). When only the position states are considered, this numerical integration then includes 102 first-order, coupled differential equations for computation of the series, using 32-terms for each of the position states.

A comparison of the numerical output with the 32-term Fourier series representations for the spatial coordinates shows variation up to several thousand kilometers. Consistent with Richardson, the series representations for the velocity states were initially computed by taking the first time derivatives of the Fourier series for the position coordinates. This method leads to a nominal path that is different in position and velocity from the results seen in the numerical output. Differences up to several thousand kilometers in each of the position states were considered unacceptable and provoked further investigation into curve-fitting techniques.[14] As one alternative, the number of terms in each series could be increased and the coefficients for the nominal velocity states could be numerically integrated to improve accuracy, but this technique would add to an already high computational burden. Also, by selecting 2L to be the full duration of the orbit, the half-period will be so large that the first several coefficients of each series will not significantly contribute to the series solution. Some of these terms could, consequently, be neglected; however, another method, such as least squares, might provide closer agreement with the numerical output and could lesson the computational requirements.

B. Least Squares Curve Fits

The least squares approach constructs the "best" curve through a set of points in the sense of minimizing the sum of the squared errors in the locations of the points relative to the curve. This powerful method has had many contributors, a few of which are mentioned here. The Babylonians set the stage for the development of the method of least squares by using a rudimentary form of the Fourier series for estimation problems; then in 1632, Galileo Galilei first attempted to minimize various functions of estimation errors.[24] In 1795, Carl Friedrich Gauss invented and used the method of least squares when he was just 18 years old.[23] Adrien-Marie Legendre independently invented and first published his least squares development in 1806.[23'] The least squares approach was also developed independently in America by R. Adrain in 1808.[24] Gauss employed his least squares techniques in an orbit measurement problem and developed data processing methods for dealing with random variables.[25] In order to help astronomers locate the asteroid Ceres, Gauss invented a recursive (sequential) least squares procedure to handle the vast calculations that were necessary.[24] New data could then be added sequentially rather than the problem being recalculated with the complete batch of data when one new observation arrived.

The task of finding representations for the numerical output can be viewed as the problem of fitting six "best" curves through the six given sets of points: $(t, x(t))$, $(t, y(t))$, $(t, z(t))$, $(t, \dot{x}(t))$, $(t, \dot{y}(t))$, and $(t, \dot{z}(t))$. (The dot denotes the first derivative with respect to characteristic time.) The method of least squares can be used for this purpose. Initially, the basis functions that are used to construct the best curve through the data points must be selected. This choice of basis functions is usually made by using some hypothesized relationship for the variables as functions of time or through an analysis of a plot of the points. A set of observations of $x(t)$ at distinct times t_1, t_2, ..., t_m is assumed. Suppose that $x(t)$ can best be represented by a linear combination of n basis functions. These basis functions could be

$$1, \ t, \ t^2, \ \ldots\ldots, \ t^n$$

or

$$1, \ \cos(t), \ \sin(t), \ \cos(2t), \ \sin(2t), \ \ldots\ldots$$

Choosing basis functions that are orthogonal can lessen the possible numerical difficulties encountered later due to dependencies; however, in many cases, this is not necessary. One orthogonal choice could be Legendre polynomial $(P_0, \ \ldots, \ P_n)$ where the polynomial basis $(1, \ t, \ t^2, \ \ldots, \ t^n)$ is orthogonalized using Gram-Schmidt methods to give $P_0 = 1$, $P_1 = t$, $P_2 = t^2 - 1/3$, $\ldots$. Another basis choice might be the orthogonal Chebyshev polynomials where a cosine series such as $(1, \ \cos(\theta), \ \cos(2\theta) = 2\cos^2(\theta) -1, \ \cos(3\theta) = 4 \cos^3(\theta) - 3 \cos (\theta), \ \ldots)$ is converted using a substitution "$t = \cos(\theta)$" to give $T_0 = 1$, $T_1 = t$, $T_2 = 2 t^2 -1$, $T_3 = 4 t^3 - 3 t$, $\ldots$. A third choice of ort ogonal basis functions could be the sinusoids 1, $\cos(t)$, $\sin(t)$, $\cos(2t)$, $\sin(2t)$, $\ldots$.

In general, the method can be illustrated by assuming a set of n basis functions denoted by 1, $V_1(t)$, $V_2(t)$, $V_3(t)$, $\ldots\ldots$, $V_{n-1}(t)$. Then an expression for $x(t)$ can be computed using the basis functions $V_i(t)$ and the scalar coefficients--as yet, unknown--denoted as b_i for $i = 1, \ 2, \ 3, \ \ldots \ n-1$:

$$x(t) = b_0 + b_1 V_1(t) + \ldots\ldots + b_{n-1} V_{n-1}(t) - \text{error}.$$

The term "error" is included because the approximation is not, at the outset, assumed to be exact. With m observations and with the error denoted by "e", we can write m separate equations:

$$b_0 + b_1 V_1(t_1) + \ldots + b_{n-1} V_{n-1}(t_1) - e_1 = x(t_1) = x_1$$

$$b_0 + b_1 V_1(t_2) + \ldots + b_{n-1} V_{n-1}(t_2) - e_2 = x(t_2) = x_2$$

$$b_0 + b_1 V_1(t_3) + \ldots + b_{n-1} V_{n-1}(t_3) - e_3 = x(t_1) = x_3 \qquad (2-5)$$

$$\vdots \qquad\qquad\qquad\qquad\qquad \vdots$$

$$b_0 + b_1 V_1(t_m) + \ldots + b_{n-1} V_{n-1}(t_m) - e_m = x(t_m) = x_m$$

This system (2-5) of m equations in n unknowns can be represented in a matrix equation as

$$A \bar{b} - \bar{e} = \bar{x} \qquad (2-6)$$

where

$$A = \begin{bmatrix}
1 & V_1(t_1) & V_2(t_1) & \ldots\ldots & V_{n-1}(t_1) \\
1 & V_1(t_2) & V_2(t_2) & \ldots\ldots & V_{n-1}(t_2) \\
1 & V_1(t_3) & V_2(t_3) & \ldots\ldots & V_{n-1}(t_3) \\
\cdot & \cdot & \cdot & & \cdot \\
\cdot & \cdot & \cdot & & \cdot \\
\cdot & \cdot & \cdot & & \cdot \\
\cdot & \cdot & \cdot & & \cdot \\
1 & V_1(t_m) & V_2(t_m) & \ldots\ldots & V_{n-1}(t_m)
\end{bmatrix}, \qquad (2-7)$$

34

$$\overline{b} = \begin{bmatrix} b_0 \\ b_1 \\ b_2 \\ . \\ . \\ . \\ b_{n-1} \end{bmatrix}, \qquad (2-8)$$

$$\overline{e} = \begin{bmatrix} e_0 \\ e_1 \\ e_2 \\ . \\ . \\ . \\ e_m \end{bmatrix}, \qquad (2-9)$$

and

$$\overline{x} = \begin{bmatrix} x(t_0) \\ x(t_1) \\ x(t_2) \\ . \\ . \\ . \\ x(t_m) \end{bmatrix}. \qquad (2-10)$$

35

In general, least squares problems are overdetermined (with $m > n$); an exact solution to the overdetermined system $A \bar{b} = \bar{x}$ is possible only if the error vector, $\bar{e}$, is the zero vector (all m equations hold exactly). Generally, an exact solution is not possible. There are many methods that can be used to solve an equation such as (2-6); Skelton[26] discusses several of the methods.

The least squares method minimizes the sum of the squared error terms. Since any particular error term could be positive or negative, the sum of the errors could be very small while individual errors were still quite large. Consequently, the sum of the squared errors is the cost function that is minimized. We minimize P where

$$P = \sum_{i=1}^{m} e_i^2 = \bar{e}^T \bar{e}. \qquad (2\text{-}11)$$

The overbar denotes a vector, and the "T" indicates a transpose. Using equation (2-6) in equation (2-11), the cost function simplifies to

$$P = \bar{b}^T A^T A \, \bar{b} - 2 \, \bar{x}^T A \, \bar{b} + \bar{x}^T \bar{x}. \qquad (2\text{-}12)$$

Minimizing equation (2-12) with respect to $\bar{b}$ results by taking the derivative of the scalar P with respect to the vector $\bar{b}$:

$$\frac{\partial P}{\partial \bar{b}} = A^T A \bar{b} + (\bar{b}^T A^T A)^T - 2 \, (\bar{x}^T A)^T = 0. \qquad (2\text{-}13)$$

Note that the term $\bar{x}^T \bar{x}$ in equation (2-12) is assumed to be a constant and does not appear in the derivative (2-13). Simple matrix algebra then leads to the solution

$$\hat{b} = (A^T A)^{-1} A^T \bar{x}. \qquad (2\text{-}14)$$

where $\hat{b}$ is used to denote the least squares estimate of the "best" vector of basis coefficients.

Equation (2-14) is a depiction of the solution; however, there are numerous solution methods that are more numerically stable than inversion of such a large system as A^TA in (2-14). For instance, when the columns of A are not independent (as can occur when the basis functions are not orthogonal), A^TA will not be invertible, and the psuedoinverse of A^TA can be used to complete the least squares approach.[27] Even when A^TA is invertible, the notation $(A^TA)^{-1}$ is included only to depict a solution for the unknown coefficients. Generally, a more computationally efficient and numerically stable method than matrix inversion is used. A method such as QR factorization using Gram-Schmidt methods or the use of a set of Householder transformations is more efficient than inverting A^TA.[27] In order to briefly illustrate the QR decomposition method, the matrix A^TA is written as

$$A^TA = QR$$

where Q is an orthogonal matrix such that $Q^{-1} = Q^T$ and and R is triangular and easily inverted. The least squares solution derived from equation (2-13) is

$$A^TA \, \bar{b} = A^T\bar{x}$$

Using the QR decomposition, this equation can then be written as

$$(QR)\bar{b} = A^T\bar{x}.$$

The solution

$$\hat{b} = R^{-1}Q^TA^T\bar{x}$$

involves inversion of only a diagonal matrix R.

For this work, sinusoidal basis functions were the logical choice for the states (see Figures 2-1 and 2-2). Using the x coordinate as an example, one row in the least squares formulation for the time step m can be written as

$$a_0 + a_1\cos\left(\frac{\pi t_m}{L}\right) + b_1\sin\left(\frac{\pi t_m}{L}\right) + \ldots + a_n\cos\left(\frac{n\pi t_m}{L}\right) + b_n\sin\left(\frac{n\pi t_m}{L}\right) = x_m \qquad (2\text{-}15)$$

where "L" is the half-period selected for the computation. The number of basis functions (2n+1) can be chosen to produce the most accurate representation, as well as limiting the computational burden. If 101 basis functions were desired, the "last" basis function would be $\sin\left(\frac{50\pi t_m}{L}\right)$, and its (yet to be determined) coefficient would be b_{50}. The rows representing all integration time steps can be combined in matrix form to produce the matrix equation

$$A\bar{b} = \bar{x} \qquad (2\text{-}16)$$

where A is a matrix with m rows, one for each of the m time steps, and with n columns corresponding to the number of trigonometric basis functions selected. The vector $\bar{b}$ contains the coefficients for the basis functions. The column vector $\bar{x}$ has m entries for the x coordinate, one for each of the m time steps. (Note that if curve fits for all six states were necessary, then this method would be applied six times with the right hand side of equation (2-16) being $\bar{x}$ then $\bar{y}$ and so forth. The coefficients in $\hat{b}$ determined for each state variable would consequently be different.)

The least squares approach solves for the "best" estimate, $\hat{b}$, of the vector $\bar{b}$ by minimizing the sum of the squared errors.[28] The

38

estimate $\hat{b}$ is calculated such that $\hat{x} = A\hat{b}$ differs from $\bar{x}$ by some error vector $\bar{e}$, where

$$\bar{e} = \hat{x} - \bar{x}, \qquad (2\text{-}17)$$

and the least squares estimate that results is

$$\hat{b} = (A^T A)^{-1} A^T \bar{x}. \qquad (2\text{-}18)$$

The scalar entries in the vector $\hat{b}$ are then the Fourier coefficients for the basis functions selected for use in the formulation.[27] This approach to calculating the coefficients of the sinusoidal basis functions has the advantages of computational efficiency and great flexibility in the choices of fundamental period, 2L, and the number of basis functions, 2n+1, retained in the series.[29] By choosing basis functions that are orthogonal, possible numerical difficulties due to dependencies can be eliminated, and the independent contribution of each basis function can be judged by the relative size of its coefficient.

Two criteria are used here to compare the various options for the fundamental period and the number of basis functions. The value of the sum of the squared errors $(\bar{e}^T \bar{e})$ can be calculated in order to compare various choices of n and L. The element of the error vector $\bar{e}$ with the largest magnitude provides an indicator of the maximum error for a specific choice of n and L, and it is denoted as e_{max}. The scalars e_{max} can also be used as a criteria for evaluating various combinations of n and L. The error vector is calculated by noting that

$$\bar{e} = \hat{x} - \bar{x} = A\hat{b} - \bar{x} = A(A^T A)^{-1} A^T \bar{x} - \bar{x} = [A(A^T A)^{-1} A^T - I]\,\bar{x} \qquad (2\text{-}19)$$

The identity matrix is denoted as I. The value e_{max} is then defined as the entry in the vector $\bar{e}$ that has the largest absolute value. In one

39

evaluation of this method, a Lissajous orbit of approximately 5 years duration was used.

The quasi-periodic nature of the Li.·sajous orbit allowed some flexibility in the choice of "period" for modeling. In one trial, a half-period of L = 87.5 days was roughly estimated from an analysis of the plot of x(t) versus time. Other values of L close to 87.5 days were also used in separate simulations, and the criteria involving determination of $\overline{e^T e}$ and e_{max} were evaluated. A half-period equal to the duration of the orbit (L = 1741.5 days) was also used and was expected to minimize the error vector magnitude for "large" values of n.[29] Over numerous trials, the best curve fit was obtained for the combination L = 1741.5 days and n = 101. The results of several simulations are presented in Table 2-1.

TABLE 2-1: COMPARISON OF LEAST SQUARES CURVE FITS

n	L = 87.5 Days		L = 1741.56386 days	
	e_{max}(km)	$e^T e$ (km^2)	e_{max}(km)	$e^T e$(km^2)
101	6.4866 X 10^3	4.9455 X 10^9	2.7262 X 10^2	1.5307 X 10^7
81	6.4805 X 10^3	4.9455 X 10^9	2.7095 X 10^2	1.7092 X 10^7
61	6.4753 X 10^3	4.9456 X 10^9	1.3447 X 10^3	6.6568 X 10^7
41	6.4820 X 10^3	4.9457 X 10^9	3.0322 X 10^3	1.6871 X 10^9
31	6.4750 X 10^3	4.9457 X 10^9	6.8196 X 10^3	3.8327 X 10^9
21	6.4930 X 10^3	4.9459 X 10^9	6.9039 X 10^3	1.0044 X 10^{12}
11	6.5635 X 10^3	4.9495 X 10^9	6.3270 X 10^4	1.2776 X 10^{12}
3	7.5111 X 10^3	5.4017 X 10^9	5.9449 X 10^4	1.3569 X 10^{12}

Clearly, using 101 basis functions for x(t), y(t), z(t), ẋ(t), ẏ(t), and ż(t) could be computationally expensive. Implementing this method with n = 101 still resulted in maximum errors (e_{max}) in the range of hundreds of kilometers in the x estimate. Errors of such a

magnitude provided improved accuracy over a 32-term series with numerically integrated Fourier coefficients, yet it was desired to further reduce the errors and the computational burden, if possible. Therefore, the third curve-fitting method attempted was weighted least squares.

C. Weighted Least Squares

The method of weighted least squares allows the introduction of weighting factors for the errors. The "most important" errors are weighted more heavily (relative to the other errors), and the weighted sum of the squared errors is minimized. Gauss developed and first used weighted least squares.[27,30] He selected a weighting scheme for the errors that allowed his weighted least squares procedure to provide a linear, unbiased, minimum variance estimate, and these properties will be used in the derivation of a state estimation algorithm described later.

Regardless of how it is determined, the weighting matrix, W, is multiplied by the error vector, $\bar{e}$, and the quantity $[W\bar{e}]^T[W\bar{e}]$ is minimized.[28] This minimization leads to the estimate

$$\hat{c} = (A^TW^TWA)^{-1}A^TW^TW\bar{x}. \qquad (2\text{-}20)$$

Several weighting schemes were considered. Comparison of the least squares curve fits with the numerical output revealed that the poorest agreement of the curve with the numerical data occurred in the ranges where the $x(t)$ position coordinate was near its maximum value. In one trial, therefore, the errors associated with data points for which the values of $x(t)$ were near their maximum magnitude were given a relatively large weight. The goal was to force the least squares curve through these points. A second trial involved a two-step process. Initially, an unweighted least squares procedure was completed. The elements of the error vector (and a function of $\bar{e}$ for some trials) were used in step two as he diagonal entries of the weighting matrix. The

41

sum of the squared errors ($\bar{e}^T\bar{e}$) and the value of e_{max} did not significantly decrease by using these various weighted least squares approaches. In the continuing search to improve the curve fit, the fourth method used was based on a piecewise fit that forced agreement at the data points.

D. Piecewise Curve Fits

Early work using a least squares method clearly indicated that an approximate (that is, the "best" approximate) curve fit is computed based on specific criteria. When segments of about 90 days were used for least squares curve fits, excellent results were obtained; this directly led to the idea of using piecewise curve fit methods for the data spanning a complete trajectory. Curve fitting using local cubic polynomials computed in a "spline" algorithm was the final method investigated.

Although tne antecedents of splines appeared in the technical literature more than 4 decades ago, it is generally agreed that the formal birth of splines was in the 1940s, and the development is closely associated with Professor I. J. Schoenberg.[31] The simplest type of spline is a set of straight lines connecting consecutive data poinis. Other types of splines might be nonlinear with rational functions, exponentials, algebraic functions, or even some piecewise combination of these functions used for a specific problem. The cubic spline approximates the position of a flexible thin beam, or draftsman's spline, passing through all the points of a given data set. In this sense, it has been found that a particular type of cubic polynomial spline nearly minimizes the strain energy over all function curves passing through the given data set.[32] This was the reason behind Schoenberg's choice of the word "spline."[32,33]

A cubic polynomial between any two data points has four degrees of freedom (four coefficients). So, for a cubic spline with m segments, the total possible degrees of freedom would be 4m. Boundary conditions for the spline segments can greatly simplify the solution. Position matching at all m data points, slope continuity, curvature continuity,

and end point slope or curvature boundary conditions result in a system of equations with a tri-diagonal $(m-2)\times(m-2)$ coefficient matrix. The resulting matrix equation can be speedily solved and stored as an array of break points (intersections) and an array of associated polynomial coefficients, both available for easy access.[32]

A simple example can illustrate both the computation of the spline coefficients and, in particular, the use of boundary conditions. Suppose a set of 5 points is given:

$$(t_1, x(t_1)) = (t_1, x_1)$$

$$(t_2, x(t_2)) = (t_2, x_2)$$

$$(t_3, x(t_3)) = (t_3, x_3)$$

$$(t_4, x(t_4)) = (t_4, x_4)$$

$$(t_5, x(t_5)) = (t_5, x_5)$$

It is assumed that these points are both the given set of five data points and the points of intersection of four cubic polynomials. This assumption is not in general necessary and is made here only for simplicity. Each segment has a polynomial of the form

$$x_i(t) = a_i(t-t_i)^3 + b_i(t-t_i)^2 + c_i(t-t_i) + d_i \quad \text{for } i = 1, 2, 3, 4. \quad (2-21)$$

The first and second derivatives with respect to time are then given by

$$\dot{x}(t) = 3a_i(t-t_i)^2 + 2b_i(t-t_i) + c_i \quad (2-22)$$

and

43

$$\ddot{x}(t) = 6a_i(t-t_i) + 2\ b_i. \qquad (2-23)$$

For notational simplicity, if $(t_{i+1} - t_i) = h_i$ and $\ddot{x}(t_i) = S_i$, then for segment i with endpoints (t_i, x_i) and (t_{i+1}, x_{i+1})

$$x_i = a_i(t_i-t_i)^3 + b_i(t_i-t_i)^2 + c_i(t_i-t_i) + d_i$$

$$= d_i, \qquad (2-24)$$

$$\dot{x}_i = 3a_i(t_i-t_i)^2 + 2b_i(t_i-t_i) + c_i$$

$$= c_i, \qquad (2-25)$$

$$\ddot{x}_i = 6a_i(t_i-t_i) + 2b_i$$

$$= 2b_i = S_i, \qquad (2-26)$$

$$x_{i+1} = a_i(t_{i+1}-t_i)^3 + b_i(t_{i+1}-t_i)^2 + c_i(t_{i+1}-t_i) + d_i$$

$$= a_i h_i^3 + b_i h_i^2 + c_i h_i + d_i, \qquad (2-27)$$

$$\dot{x}_{i+1} = 3a_i(t_{i+1}-t_i)^2 + 2b_i(t_{i+1} - t_i) + c_i$$

$$= 3a_i h_i^2 + 2b_i h_i + c_i, \qquad (2-28)$$

and

44

$$\ddot{x}_{i+1} = 6a_i(t_{i+1} - t_i) + 2b_i$$

$$= 6a_i h_i + 2b_i = S_{i+1}. \tag{2-29}$$

Using equation (2-26),

$$b_i = S_i/2; \tag{2-30}$$

using equations (2-26) and (2-29),

$$a_i = (S_{i+1} - S_i)/6h_i; \tag{2-31}$$

finally, using equation (2-24),

$$d_i = x_i. \tag{2-32}$$

Then, placing these identities into equation (2-27), the solution

$$c_i = (x_{i+1} - x_i)/h_i - (2h_i S_i + h_i S_{i+1})/6 \tag{2-33}$$

is derived. Using the condition that the slopes from each side at all the interior points (2, 3, and 4) must match and modifying equation (2-28) for the i-1 point,

$$\dot{x}_i = c_i = \dot{x}_{i-1}$$

$$= 3a_{i-1}(h_{i-1}^2) + 2b_{i-1}\, h_{i-1} + c_{i-1}. \qquad (2\text{-}34)$$

Expressions for a_{i-1}, b_{i-1}, and c_{i-1} can be readily obtained from equations (2-31), (2-30) and (2-33), respectively. These expressions can then be substituted into equation (2-34), and the resulting expression can be equated to (2-33). An equation in the unknowns S_{i-1}, S_i, S_{i+1} and in the given values x_i, x_{i-1}, h_{i-1}, and h_i is then obtained (after some algebra):

$$h_{i-1}\, S_{i-1} + 2(h_{i-1} + h_i)\, S_i + h_i S_{i+1} =$$

$$6[(x_{i+1}-x_i)/h_i - (x_i-x_{i-1})/h_{i-1}] \qquad (2\text{-}35)$$

For this specific example, equation (2-35) can be used at the three interior points where cubic polynomials intersect to give,

for $i=2$,

$$h_1 S_1 + 2(h_1+h_2)\, S_2 + h_2 S_3 = 6[(x_3-x_2)/h_2 - (x_2-x_1)/h_1] = x_2,$$

for $i=3$,

$$h_2 S_2 + 2(h_2+h_3)\, S_3 + h_3 S_4 = 6[(x_4-x_3)/h_3 - (x_3-x_2)/h_2] = x_3,$$

and, for $i=4$,

$$h_3 S_3 + 2(h_3+h_4)\, S_4 + h_4 S_5 = 6[(x_5-x_4)/h_4 - (x_4-x_3)/h_3] = x_4.$$

Boundary conditions are used to find S_1 and S_5 for this 5-point problem. These conditions could be $S_1 = S_5 = 0$; this choice results in what is called a "natural" spline. Alternatively, the "not-a-knot" end conditions are present if the end point derivatives are not specified and the required polynomial pieces are reduced from n-1 to n-3. For the following example, the end point second derivatives are chosen such that $S_1 = S_2$ and $S_5 = S_4$. The final result is an (n-2) x (n-2) or, in this case, a 3 x 3 tri-diagonal system:

$$
\begin{bmatrix}
3h_1 + 2h_2 & h_2 & 0 \\
h_2 & 2h_2 + 2h_3 & h_3 \\
0 & h_3 & 2h_3 + 3h_4
\end{bmatrix}
\begin{bmatrix}
S_2 \\
S_3 \\
S_4
\end{bmatrix}
=
\begin{bmatrix}
x_2 \\
x_3 \\
x_4
\end{bmatrix}.
\qquad (2\text{-}36)
$$

Equation (2-36) can be written in more compact form as

$$A \, \overline{S} = \overline{x}$$

Solving for the unknowns S_2, S_3, and S_4 then allows solution of equations (2-31) through (2-33) for the coefficients a_i, b_i, c_i, and d_i for each of the polynomial segments. The cubic spline, with curvature continuity, can then be stored as an array of break points (intersections) and an array of associated polynomial coefficients for easy access and interpolation.

The boundary conditions at points 1 and n could have been altered to stipulate the slopes at these endpoints. When these slopes are known due to some prior knowledge of the data set, the resulting cubic spline with curvature continuity and with slope boundary conditions is called a "complete" cubic spline. It has been determined that a complete cubic spline interpolant approximately minimizes the strain energy over all function curves passing through the given data set.

47

Following a review of cubic spline interpolants and the use of some of these splines to fit a representative data set, a method devised by Hiroshi Akima[34] deserves special mention. The Akima spline minimizes extraneous points of inflection and provides a smooth curve that closely resembles one that could be drawn manually through the data. The Akima spline interpolation routine produced excellent results for the state coordinates associated with a Lissajous trajectory. It was exact through all modeled points, consistent with its formulation.

The most unique characteristic of the Akima spline is that it combats "wiggles" in the interpolant curve by minimizing extraneous points of inflection. In this way, the Akima spline provides a smooth curve that closely resembles one that would be drawn manually through the data set. Several mathematical methods for interpolating a single valued function result in a curve that is very different than the smooth curve that would be drawn manually. Methods that place polynomial or another type of curve through a data set, and even some splines, generally produce unnatural points of inflection.[34] It can be shown that there is a unique polynomial of degree n through n+1 points or a unique trigonometric polynomial with n terms through n−1 points.[35] Figures 2-3, 2-4, and 2-5 illustrate the use of a ten degree polynomial, 11-term sinusoidal curves, and spline approximations, respectively, passing through the 11 points listed in Table 2-2.[34] Extra "wiggles" (points of inflection) are obvious in Figures 2-3 and 2-4. The spline approximations in Figure 2-5 are not Akima splines, and they do exhibit an additional point of inflection near t=6.

TABLE 2-2. LIST OF POINTS USED IN THE COMPARISONS OF METHODS

t	0	1	2	3	4	5	6	7	8	9	10
x(t)	10	10	10	10	10	10	10.5	15	50	60	85

Using a 10-Degree Polynomial Fit
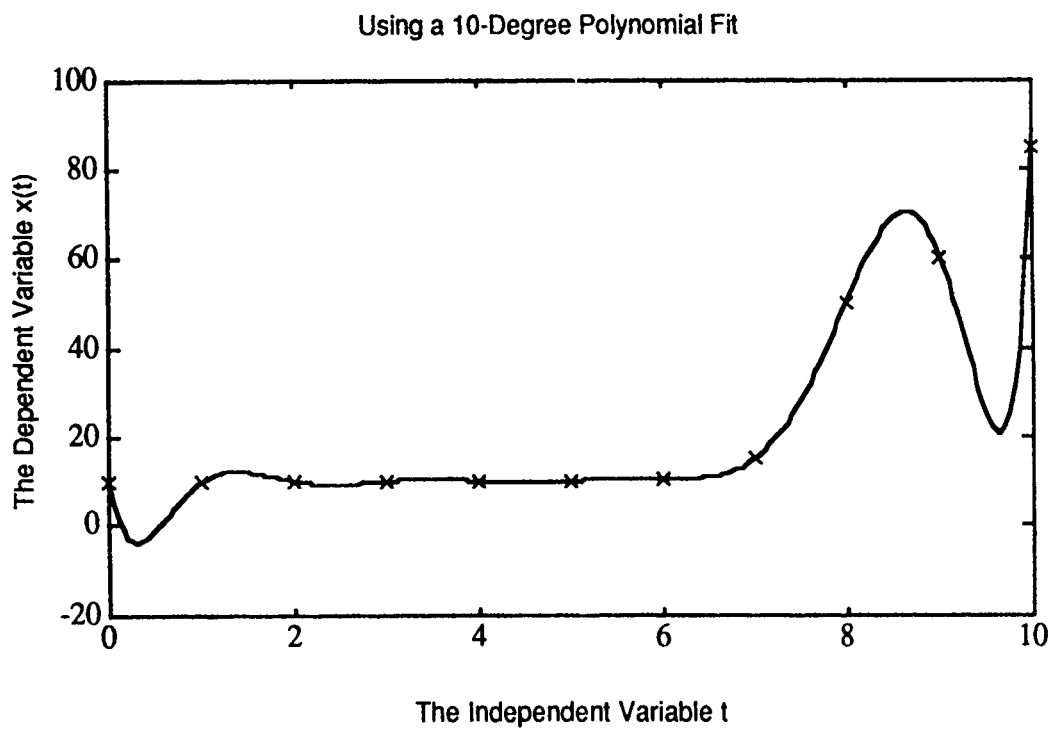
Figure 2-3. Using a 10-Degree Polynomial Curve Fit.

Using an 1'1-Term Sine Series Fit

The Dependent Variable x(t)

The Independent Variable t

Using an 11-Term Cosine Series Fit

The Dependent Variable x(t)

The Independent Variable t
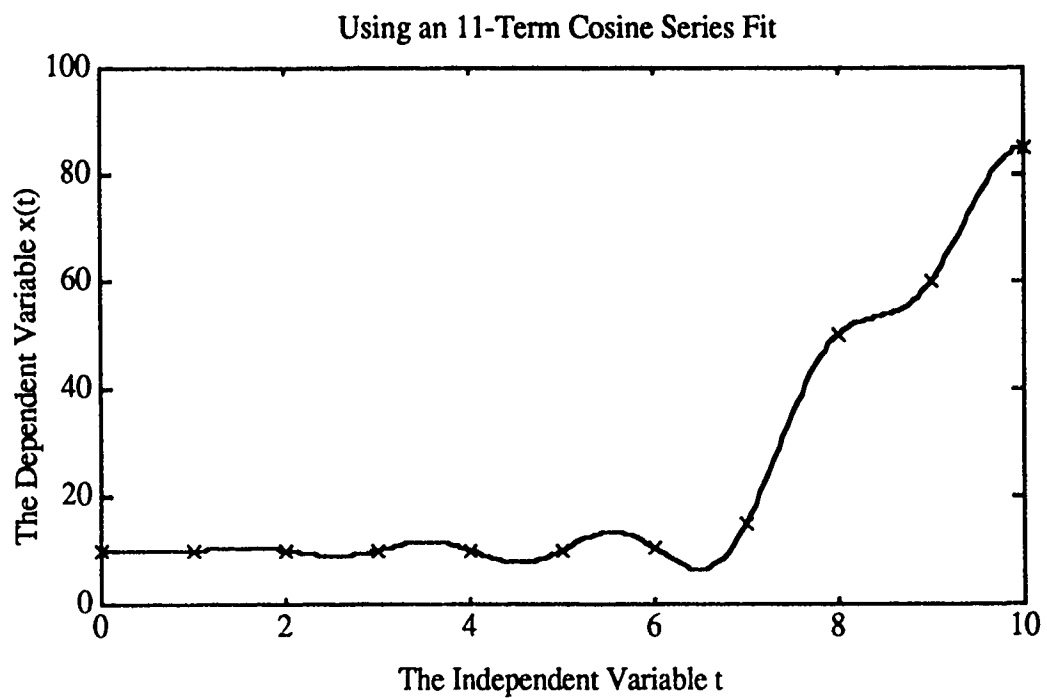
Figure 2-4. Using a Sinusoidal Fit.

Using a Cubic Spline Curve Fit with "Not-A-Knot" End Conditions

Using a Cubic Spline with "Natural" End Conditions
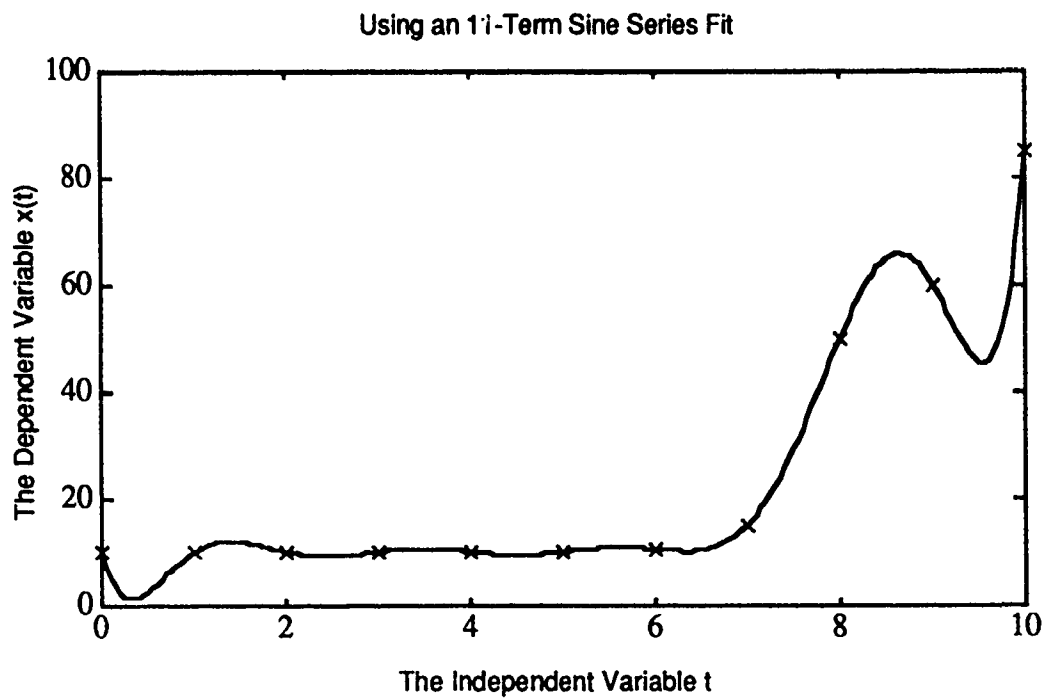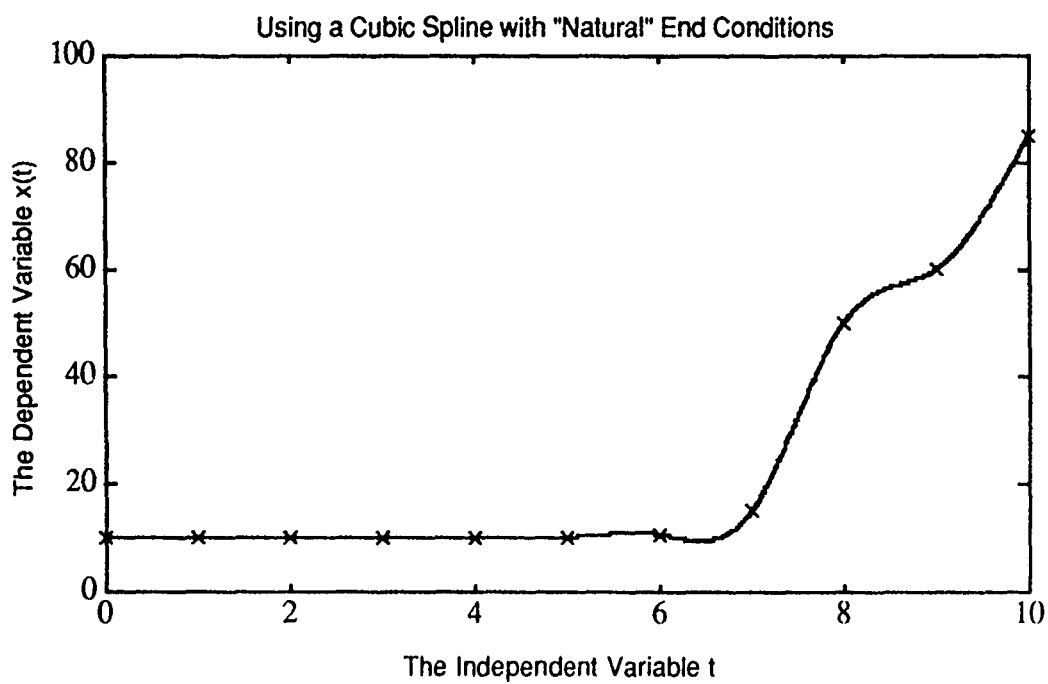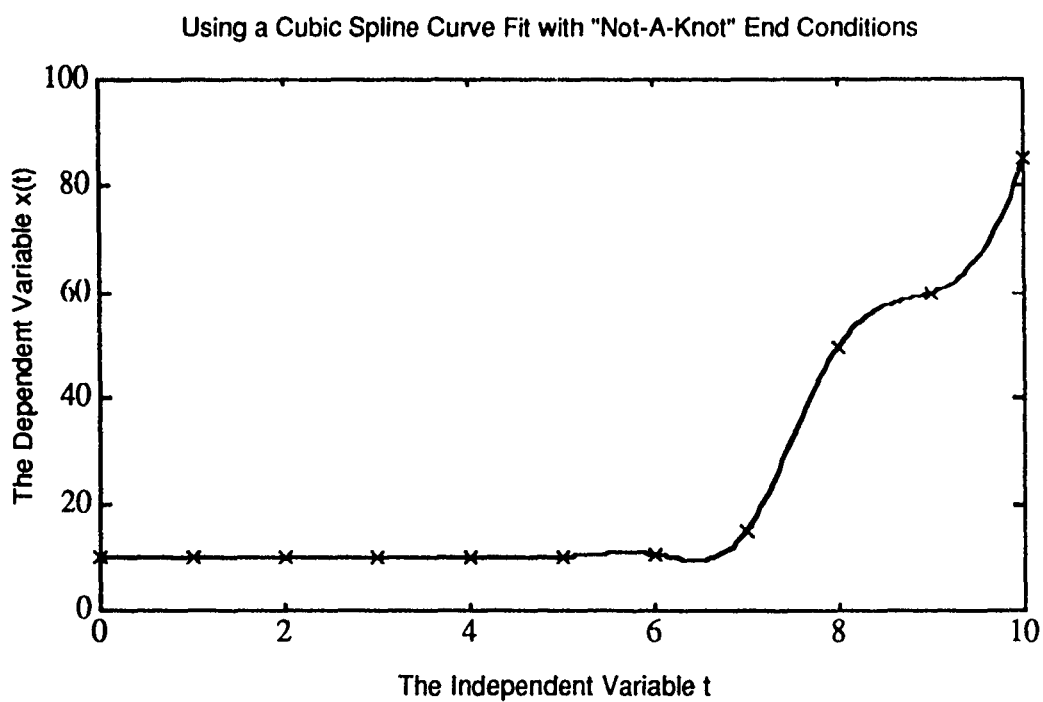
Figure 2-5. Using a Cubic Spline Curve Fit.

The Akima spline relies on locally determined slopes using geometrical relationships at each junction point. A spline in general removes the global dependence of a polynomial on some remote local properties: if the function to be approximated by a polynomial is badly behaved anywhere in the interval of approximation, then the approximation is poor everywhere.[33] The Akima spline goes one step further, beyond removing global dependence, by also calculating local slopes from the data set and matching these at each junction point. The method uses five points P_{i-2}, P_{i-1}, P_i, P_{i+1}, P_{i+2} selected from the data set to calculate the slope at point P_i.[34] Boundary conditions are provided by estimating two more points on each end of the data set and then calculating the slopes at the end points. For every five points, the slopes of the four line segments $\overline{P_{i-2}P_{i-1}}$, $\overline{P_{i-1}P_i}$, $\overline{P_iP_{i+1}}$, and $\overline{P_{i+1}P_{i+2}}$ are denoted by M_1, M_2, M_3 and M_4, respectively. The geometrical relationships used by Akima lead to an expression of the slope at point P_i (denoted as t_i):[34]

$$t_i = \frac{((|M_4 - M_3|)M_2 + (|M_2 - M_1|)M_3)}{(|M_4 - M_3| + |M_2 - M_1|)}.$$

When the denominator of t_i is zero, this slope at point P_i is given by

$$t_i = (1/2)(M_2 + M_3)$$

Thus, position and slope are specified at each data point, and between any two data points, four conditions are present. A third-order polynomial can then be uniquely determined.

The Akima algorithm and several other spline interpolation routines produced excellent results for the coordinates of a libration point Lissajous trajectory and required very little computational memory. While the Akima spline in general produces a curve fit with a minimal number of points of inflection, the reference trajectories used in this effort are relatively easy to curve fit with a either a

"natural" or "not-a-knot" cubic spline. Routines available in 386-Matlab[32] are used primarily in this research effort.

Several differing spline routines generated excellent curve fits. The computation incorporates forced agreement at all modeled data points; however, analysis of the curve fit between data points is then necessary. That is, it would be interesting to question how accurately the cubic spline models the actual orbit between data points. A typical numerical data set for a 800-day Lissajous trajectory was selected to evaluate the shape-preserving nature of the spline. Every other point of the data set was removed and stored for later comparison. An Akima spline was then computed through the remaining points. This spline was used to predict the locations of the points that had been removed, and the spline prediction was compared to the actual values. The results showed errors, when using an Akima cubic spline, of less than one kilometer for the interior spline points. Similar tests using other cubic spline routines also showed errors of consistently less than one kilometer; the results are summarized in Table 2-3 and Figure 2-6 . In most cases, the difference between the spline-computed positions and the positions of the removed points were less than .5 kilometers. The difference in accuracy delivered by the Akima or a more general cubic spline is much better (in meters) if the corresponding numerical data is available for time steps of approximately 2 days or less.

Table 2-3. Curve Fit Accuracy Using Cubic Splines
for the x(t) Coordinate of a Lissajous Path.

|	
Orbit Duration	802.9063 days
Average integration time step	2.8400 days
Average change in x(t) during the time step	4255.0000 km
Minimum x(t) coordinate value	388.2521 km
Maximum x(t) coordinate value	56078.0000 km
Maximum error at unmodeled points using natural spline	.6182 km
Maximum error at unmodeled points using not-a-knot spline	.6181 km
Maximum error at modeled points using natural spline	0 km
Maximum error at modeled points using not-a-knot spline	0 km
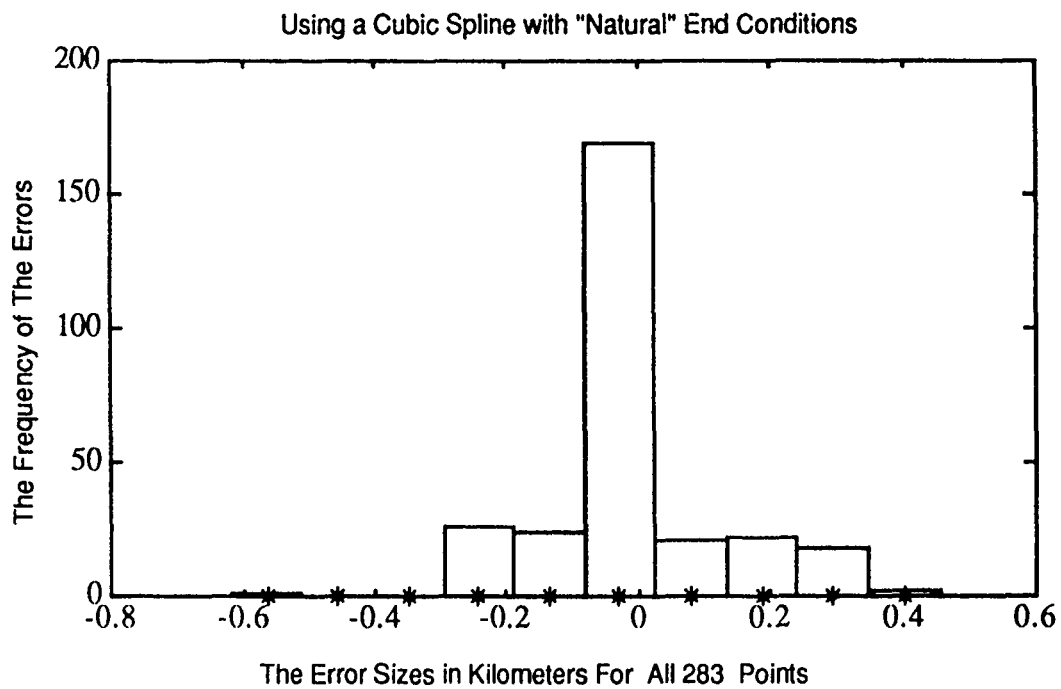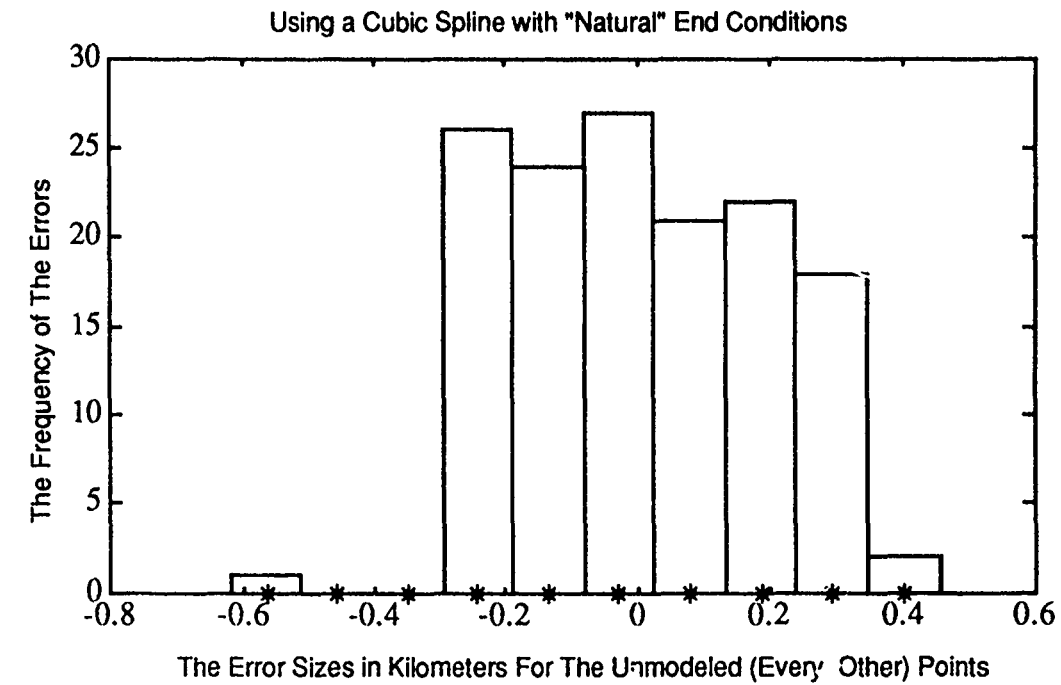
Figure 2-6. Histograms of Errors Caused by Curve Fitting
a Lissajous Path Using Cubic Splines when
Every Other Point is Unmodeled.

The cubic spline has proven to be a useful and accurate interpolating polynomial for the coordinates of a Lissajous trajectory about the interior libration point. Fourier series and least squares approaches using trigonometric polynomials could not match its accuracy; computation and storage do not seem to present a problem when cubic splines are used to represent the nominal trajectory.

Cubic splines, including the Akima spline, were used in the subsequent work for the computation of the numerical entries in the Jacobian matrix as it was evaluated along the nominal path, and for the calculation of residuals relative to the reference trajectory. When range and range-rate measurements are simulated, the nonlinear measurement equations are commonly linearized about the nominal path. The cubic spline can then also be used to compute the time-varying entries in the resulting measurement matrix. The Akima cubic spline software is available in the International Mathematical and Statistical Libraries (IMSL) by using the routines CSAKM (to compute the spline) and CSVAL (to evaluate the spline at a specified abscissa value). A useful cubic spline program is also available on 386-Matlab[32] by using the SPLINE (computation) and PPVAL (evaluation) routines. The routines CSAPN and CSAPI can also be used in Matlab to construct natural and not-a-knot cubic splines, respectively. Spline representations can now be incorporated in both the error analysis and station-keeping studies in future research.

CONCLUSION

The restricted three-body problem is an important and interesting area of research. The Sun-Earth+Moon ER3BP, in particular, is currently an area of vital research attention. The use of highly accurate, numerically integrated nominal trajectories, coupled with the need of a continuous representation of the path, necessitates the investigation of curve fit methods. Other researchers have used approximate Fourier series representations to curve fit the numerically integrated libration point orbits. The use of such an approximate curve near an accurately determined, numerically integrated path seems, in part, to be wasted numerical integration effort. Other researchers working on European Space Agency missions, have used tabular look-up methods (linear interpolation) as a curve fit method. This approximation ignores the curvature of the data, regardless of the duration of the time steps used in the numerical integration. The curve fitting using cubic splines exactly models every data point from the numerical integration routine, accurately models the curvature between the data points, and is computationally efficient. Simulations used to compute the state transition matrix and linearized measurement equations and to calculate expected tracking errors and the cost of maintaining the spacecraft near the unstable orbits can now also incorporate cubic spline curve fits. This , in turn, will improve the accuracy of further studies conducted in relation to future spacecraft missions.

LIST OF REFERENCES

1. S.C. Gordon, "Some Results of Adding Solar Radiation Pressure Forces to the Restricted Three-Body Problem," USAFA TR 91-10, September 7, 1991.

2. R.W. Farquhar, "The Control and Use of Libration-Point Satellites," Ph.D. Dissertation, Department of Aeronautics and Astronautics, Stanford University, Stanford, California, July 1968.

3. R.W. Farquhar, "A Halo-Orbit Lunar Station," *Astronautics and Aeronautics*, June 1972, pages 59-63.

4. J.R. Wertz, Editor, *Spacecraft Attitude Determination and Control*, D. Reidel Publishing Co, Boston, 1978.

5. S. Wolf, *Guide to Electronic Measurements and Laboratory Practice*, Prentice Hall, Englewood Cliffs, New Jersey, 1973.

6. R.W. Farguhar and A.A. Kamel, "Quasi-Periodic Orbits About the Translunar Libration Point," *Celestial Mechanics*, Volume 7, 1973, pages 458- 473.

7. D.L. Richardson and N.D. Cary, "A Uniformly Valid Solution for Motion About the Interior Libration Point of the Perturbed Elliptic-Restricted Problem," AAS/AIAA Astrodynamics Specialists Conference, Nassau, Bahamas, July 28-29, 1975, AAS Paper 75-021.

8. D.L. Richardson, "Halo Orbit Formulation for the ISEE-3 Mission," *Journal of Guidance and Control*, Volume 3, Number 6, November-December 1980, pages 543-548.

9. H.J. Pernicka, "The Numerical Determination of Nominal Libration Point Trajectories and Development of a Station-Keeping Strategy.' PhD Dissertation, School of Aeronautics and Astronautics, Purdue University, West Lafayette, Indiana, May 1990.

10. H.J. Pernicka, "The Numerical Determination of Lissajous Orbits in the Circular Restricted Three-Body Problem," M.S. Thesis, School of Aeronautics and Astronautics, Purdue University, West Lafayette, Indiana, December 1986.

11. K.C. Howell and H.J. Pernicka, "Numerical Determination of Lissajous Trajectories in the Restricted Three-Body Problem," *Celestial Mechanics*, Volume 41, 1988, pages 107-124.

12. K.C. Howell, Principal Investigator, "Trajectory Design for Libration Point Trajectories and for Double Lunar Swingby Trajectories," Final Report Prepared for Computer Sciences Corporation, December 1987.

13. K.C. Howell, Principal Investigator, "Design of Libration Point Trajectories and Consecutive Lunar Encounter Trajectories," Final Report Prepared for Computer Sciences Corporation, September 1988.

14. H.J. Pernicka, "The Numerical Determination of Libration Point Trajectories, Including Development of Station-Keeping Strategies," Proposal for Dissertation, School of Aeronautics and Astronautics, Purdue University, West Lafayette, Indiana, December 1988.

15. J.L. Bell, Private Communication, School of Aeronautics and Astronautics, Purdue University, West Lafayette, Indiana, August, 1990.

16. The MathWorks, *386-Matlab*, 21 Eliot Street, South Natick, Ma, 1989.

17. V. Szebehely, *Theory of Orbits: The Restricted Problem of Three Bodies*, Academic Press, New York, 1967.

18. A.E. Roy, *Orbital Motion*, Second Edition, Adam Hilger Ltd, Bristol, England, 1982.

19. E.A. Grebenikov, "On the Stability of the Lagrangian Triangle Solutions of the Restricted Elliptic Three-Body Problem," *Soviet Astronomy*, Volume 8, Number 3, November-December 1964, pages 567-578.

20. J.M.A. Danby, "Stability of the Triangular Points in Elliptic Restricted Problem of Three Bodies," *The Astronomical Journal*, Volume 69, Number 2, March 1964, pages 165-172.

21. A. Bennett, "Characteristic Exponents of the Five Equilibrium Solutions in the Elliptically Restricted Problem," *Icarus*, Volume 4, 1965, pages 177-190.

22. D.L. Richardson, "Analytic Construction of Periodic Orbits About the Collinear Points," *Celestial Mechanics*, Volume 22, 1980, pages 241-253.

23. R.H. Battin, *An Introduction to the Mathematics and Methods of Astrodynamics*, AIAA Education Series, New York, 1987.

24. T. Kailath, "A View of Three Decades of Linear Filtering Theory," *IEEE Transactions on Information Theory*, Volume IT-20, Number 2, March 1974.

25. A. Gelb, Editor, *Applied Optimal Estimation*, The M.I.T. Press, Cambridge, Massachusetts, 1974.

26. R.E. Skelton, *Dynamic System Control*, John Wiley and Sons, New York, 1988.

27. G. Strang, *Introduction to Applied Mathematics*, Wellesly-Cambridge Press, Wellesley, Massachusetts, 1986.

28. G. Strang, *Linear Algebra and its Applications*, second edition, Academic Press, Orlando, Florida, 1980.

29. F.B. Hildebrand, *Introduction to Numerical Analysis*, McGraw-Hill Book Company, New York, 1956.

30. B.D. Tapley, V. Szebehely, Editors, *Recent Advances in Dynamical Astronomy*, B.D. Tapley, "Statistical Orbit Determination Theory," D. Reidel, Dordrecht-Holland, 1988, pages 396-425.

31. H. Werner, "The Development of Non Linear Splines and Their Applications," *Approximation Theory III*, E.W. Cheney, editor, Academic Press, New York, 1980, pages 125-150.

32. C.F. Gerald, P.O. Wheatley, *Applied Numerical Analysis*, third edition, Addison-Wesley, Reading, Massachusetts, 1985.

33. C. de Boor, *A Practical Guide to Splines*, Springer-Verlag, New York, 1978.

34. H. Akima, "A New Method of Interpolation and Smooth Curve Fitting Based on Local Procedures," *Journal of the Association for Computing Machinery*, Volume 17, Number 4, October 1970, pages 589-602.

35. C.A. Micchelli, "Algebraic Aspects of Interpolation," pages 81-102, *Approximation Theory*, Volume 36, Carl deBoor, editor, American Mathematical Society, Providence Rhode Island, 1986.

END

FILMED

DATE: 10-91

DTIC